

Geology of the western margin of the Grand Forks complex, southern British Columbia: high-grade Cretaceous metamorphism followed by early Tertiary extension on the Granby fault

J.D. Laberge and D.R.M. Pattison

Abstract: The Grand Forks complex, in the southern Omineca belt of British Columbia, is a fault-bounded tectonic window exposing Proterozoic sediments and associated mafic rocks metamorphosed to upper amphibolite to granulite facies. Its western margin is marked by the Granby fault, an Eocene west-dipping, low-angle, normal fault characterized by brittle deformation. The metasediments of the Grand Forks complex consist of migmatitic paragneiss containing a peak metamorphic assemblage of garnet + cordierite + sillimanite + K-feldspar \pm biotite + quartz. Pressure–temperature conditions for this assemblage are 800 ± 35 °C and 5.8 ± 0.6 kbar (1 kbar = 100 MPa). Resorption of garnet to cordierite \pm spinel suggests nearly isothermal decompression of about 2 kbar from peak conditions, interpreted to have occurred prior to normal displacement on the Granby fault. Laser ablation U–Pb dating of monazite from the metasediments suggests a dominant episode of Late Cretaceous metamorphism at 84 ± 3 Ma, with evidence for earlier episodes of Cretaceous metamorphism at 119 ± 3 and 104 ± 3 Ma. Early Tertiary recrystallization at 51 ± 2 Ma is coeval with the emplacement of the nearby Coryell plutonic suite. In the hanging wall of the Granby fault, allochthonous sedimentary and volcanic rocks of Quesnel terrane contain mineral assemblages indicative of the upper greenschist to lower amphibolite facies. Pressure–temperature conditions are estimated at 425 ± 40 °C and 2.3 ± 0.7 kbar. The throw (vertical displacement) on the Eocene Granby fault is estimated to be on the order of 5 km. While significant, the fault cannot account for the entire amount of tectonic uplift of the core complex.

Résumé : Le complexe métamorphique de Grand Forks est une fenêtre tectonique, bordée de failles normales, qui expose des roches de la croûte moyenne dans la ceinture d'Omineca, en Colombie-Britannique. Sur sa marge occidentale, la faille éocène de Granby est une faille cassante à pendage modéré vers l'ouest. Le complexe métamorphique expose des migmatites au faciès des granulites, localement caractérisés par l'assemblage minéralogique grenat + cordiérite + sillimanite + feldspath potassique \pm biotite + quartz, dérivées de sédiments protérozoïque. Les conditions de pression–température maximum sont estimées à 800 ± 35 °C et $5,8 \pm 0,6$ kbar (1 kbar = 100 MPa). Une texture de résorption du grenat en cordiérite suggère un épisode de décompression quasi-isothermique, précédant le déplacement sur la faille de Granby. La datation U–Pb par ablation au laser sur monazite démontre une période de métamorphisme régional au Crétacé tardif à 84 ± 3 Ma. Des événements métamorphiques sont aussi datés à 119 ± 3 et 104 ± 3 Ma. Une recrystallisation éocène de la monazite (51 ± 2 Ma) est concomitante avec l'intrusion du batholithe de Coryell. Dans le toit de la faille de Granby, les roches sédimentaires et volcaniques allochtones du terrane de Quesnel contiennent des assemblages minéralogiques caractéristiques de la transition entre le faciès supérieur des schistes verts au faciès inférieur des amphibolites. Les conditions de pression–température y sont estimées à 425 ± 40 °C et $2,3 \pm 0,7$ kbar. La composante verticale du rejet sur la faille pourrait être de l'ordre de 5 km. Bien qu'importante, cette faille n'explique donc pas à elle seule le soulèvement tectonique du complexe métamorphique.

Introduction

The Grand Forks complex (GFC) in southeastern British Columbia is a tectonic window exposing mid-crustal, high-

grade, metamorphic rocks of North American affinity, in addition to a variety of younger plutonic rocks. The GFC is bounded by low-angle, outward-dipping, normal faults: the Kettle River fault to the east and the Granby fault to the

Received 17 October 2005. Accepted 13 June 2006. Published on the NRC Research Press Web site at <http://cjes.nrc.ca> on 14 April 2007.

Paper handled by Associate Editor K. Ansdell.

J.D. Laberge¹ and D.R.M. Pattison.² Department of Geology and Geophysics, University of Calgary, Calgary, AB T2N 1N4, Canada.

¹Present address: Kennecott Canada Exploration Inc., #354-200 Granville Street, Vancouver, BC V6C 1S4, Canada.

²Corresponding author (e-mail: pattison@ucalgary.ca).

west (Fig. 1). In Washington State the continuation of the complex is known as the Kettle Dome (Cheney 1980; Rhodes and Cheney 1981). The GFC is centrally located within the Shuswap culmination of the southern Omineca belt, a region of high-grade metamorphic rocks in the hinterland of the Cordilleran orogen. The evolution of the Shuswap complex involved late Mesozoic compressional deformation and Tertiary regional extension and denudation (Brown and Journeay 1987; Parrish et al. 1988). Unlike analogous core complexes, such as the Monashee complex (e.g., Johnston et al. 2000; Norlander et al. 2002; Teyssier et al. 2005) and Valhalla complex (e.g., Carr et al. 1987; Spear and Parrish 1996; Spear 2004), little work has been done on the GFC since it was mapped by Preto (1970) at a scale of 1 : 50 000. Defining the conditions and timing of the metamorphism of the core complex is needed to understand its thermotectonic evolution and to relate it to other core complexes of the Cordilleran orogen.

The west-dipping Granby fault, on the west margin of the GFC, contains Paleozoic and Mesozoic volcanic and sedimentary rocks in its hanging wall, which contrast sharply with the high-grade metamorphic rocks of the GFC in the footwall (Fig. 1). The hanging-wall rocks are interpreted to belong to the Quesnel terrane, a package of Paleozoic to Mesozoic allochthonous rocks of broadly island-arc affinity that were accreted to the western margin of North America in the Mesozoic (Monger et al. 1982; Gabrielse et al. 1991). The Granby fault is one of a number of significant Tertiary normal faults in the southern Omineca belt of British Columbia. These faults are interpreted to have accommodated a significant amount of extension during the Eocene at the end of the Cordilleran orogeny and to have strongly influenced the current crustal architecture (e.g., Price and Carmichael 1986; Brown and Journeay 1987; Parrish et al. 1988). Most of the extension on the Granby and other Eocene normal faults in the Omineca belt postdates crustal thickening and is attributed to late-orogenic gravitational collapse of an unstable, thermally weakened, thickened lithosphere (Brown and Journeay 1987; Ranalli et al. 1989; Liu and Furlong 1993).

The Granby fault strikes north-northeast and is more than 150 km in length, with 60 km of its extent north of the international border (Fig. 1). Although originally mapped as steeply dipping (Preto 1970), Carr and Parkinson (1989) locally estimated the dip of the fault at 25°–35°. A portion of the Granby fault is well exposed in the Volcanic Creek area, 15 km north of the town of Grand Forks in south-central British Columbia, near the Canada – United States border (Fig. 1). Figure 2 shows the geology of the Volcanic Creek area, based on the detailed geological mapping study of Laberge et al. (2004) and Laberge (2005).

This paper presents a study of the petrography and pressure–temperature (P – T) conditions of selected metamorphic rocks on either side of the fault in the Volcanic creek area. In addition to constraining the P – T evolution of high-grade metamorphism in the GFC, the timing of high grade metamorphism is estimated by U–Pb dating of metamorphic monazite by laser ablation – multiple collector – inductively coupled plasma – mass spectrometry (LA–MC–ICP–MS). This new information is used to better define the thermotectonic evolution of the GFC and to assess the significance of the Granby fault in

the exhumation of the GFC. The paper finishes with a brief discussion of the broader implications of these results in the context of Cordilleran lithospheric evolution.

Regional geology

The GFC is mainly composed of a high-grade metasedimentary assemblage of paragneiss, schist, quartzite, and marble, described and mapped by Preto (1970) as the Grand Forks Group. These rocks are interpreted to belong to the North American miogeocline. Amphibolite, pegmatite, orthogneiss, and granitoids are also present within the complex. All rock types are cut by late, steeply dipping, north-trending granitic to monzonitic dikes (Fig. 2). The lowest structural unit exposed in the complex, the sillimanite (Sil)-paragneiss of unit I, has been interpreted to be derived from Early Proterozoic sediments (Armstrong et al. 1991) (Table 1). Detrital zircons in the quartzite directly overlying the Sil-paragneiss give a Late Proterozoic age of 650 ± 15 Ma (Ross and Parrish 1991) (Table 1; Fig. 1), implying a major Proterozoic unconformity between the two units. The sediments, now represented by high-grade gneisses in the GFC, are therefore at least as old as Late Proterozoic to Cambrian in age. A well-defined gneissic foliation, subparallel to original bedding, gently dips towards the margin of the complex, defining a large-scale antiform (Preto 1970; Cheney 1980).

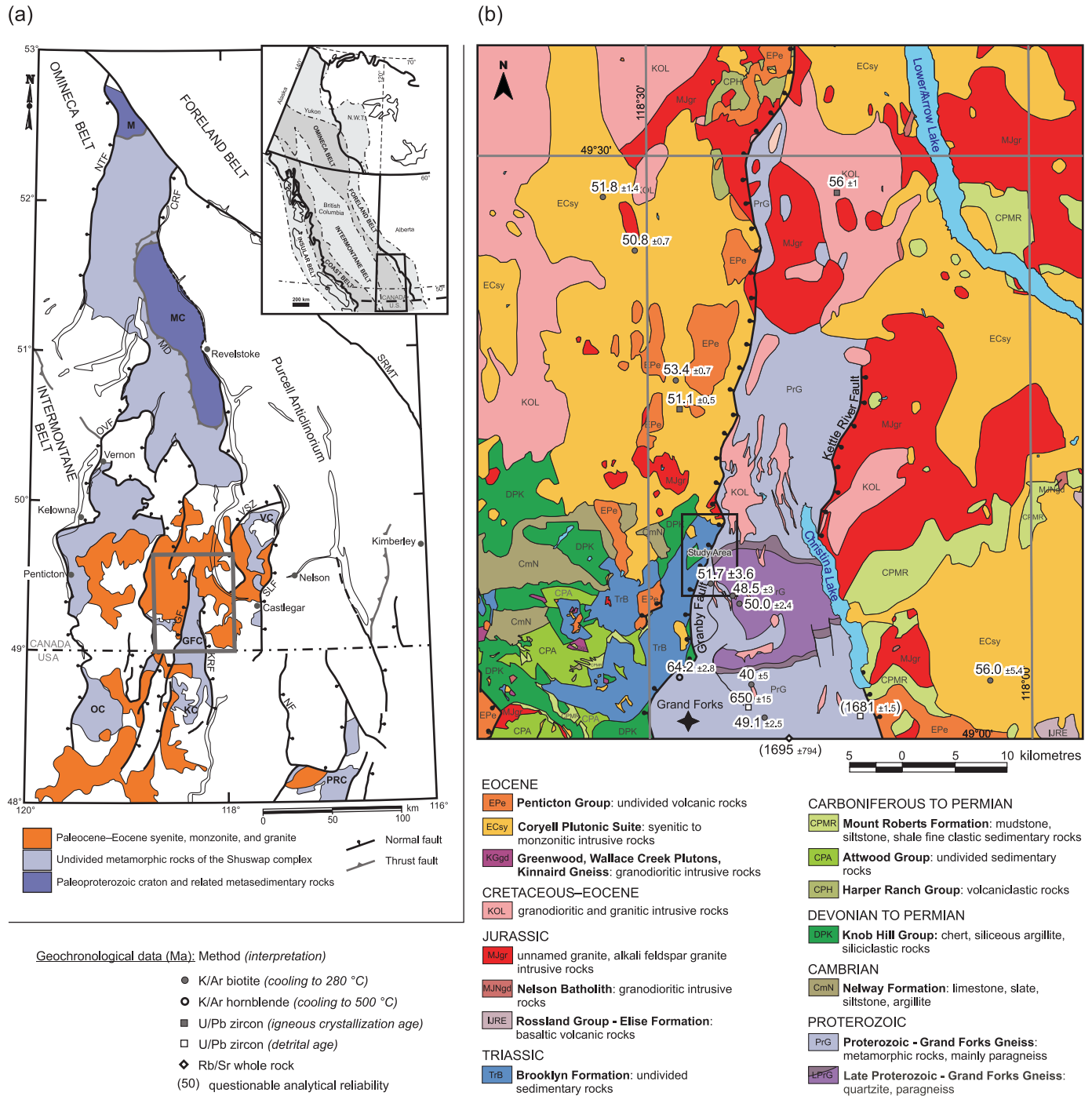
The island-arc rocks in the hanging wall of the Granby fault in the Grand Forks region consist of a sedimentary and volcanoclastic succession deposited mainly during the Cambrian to the Triassic (Fig. 1), in addition to some Jurassic volcanic rocks. There were subsequently folded, faulted, and metamorphosed to greenschist facies (Little and Thorpe 1965; Little 1983; Fyles 1990). Jurassic to Paleocene plutons of granitic to granodioritic compositions were emplaced within both footwall and hanging wall of the Granby fault. Eocene plutonic rocks of the Coryell suite and Eocene volcanic rocks of the Penticton group are the youngest units in the area, obscuring many older geological contacts (Fig. 1).

The Granby fault

In the Volcanic Creek area, the Granby fault is characterized by a zone of brittle deformation (cataclasis) in which both hanging wall and footwall rocks may be brecciated. The low-angle normal fault strikes north to north-northeast, and from its trace across topography in the map area, dips ~30° to the west (Fig. 2), consistent with the 25°–35° dip reported by Carr and Parkinson (1989) <10 km north of study area.

The strong contrast in metamorphic grade across the Granby fault suggests a significant throw. A composite cross-section drawn by Fyles (in Roback et al. 1995), suggests that the hanging wall of the Granby fault consists of a succession, some 4–6 km thick, of thrust slices repeating the Knob Hill Group and overlying Brooklyn Formation. This would require at least 4–6 vertical km of west-side-down slip on the Granby fault near Grand Forks. The Coryell syenite is, in part, cut by the Granby fault, constraining the latest movement to be post 51.1 ± 0.5 Ma (Carr and Parkinson 1989) (Table 1; Fig. 1b).

Fig. 1. Regional maps showing the location of the Grand Forks complex (GFC). (a) Simplified tectonic map of the southern Omineca belt (modified after Johnson and Brown 1996; Rhodes and Cheney 1981; Schaub et al. 2002); M, Malton gneiss; MC, Monashee complex; VC, Valhalla complex; KC, Kettle complex; OC, Okanogan complex; OVF, Okanagan Valley fault; CRF, Columbia River fault; MD, Monashee decollement; VSZ, Valky shear zone; SLF, Slocan Lake fault; GF, Granby fault; KRF, Kettle River fault; NTF, North Thompson fault; SRMT, Southern Rocky Mountain Trench. (b) Geological map around the GFC (modified from Massey et al. 2003; Preto 1970; Tempelman-Kluit 1989). Rectangular outline shows the location of Fig. 2. See web version of paper for colour.



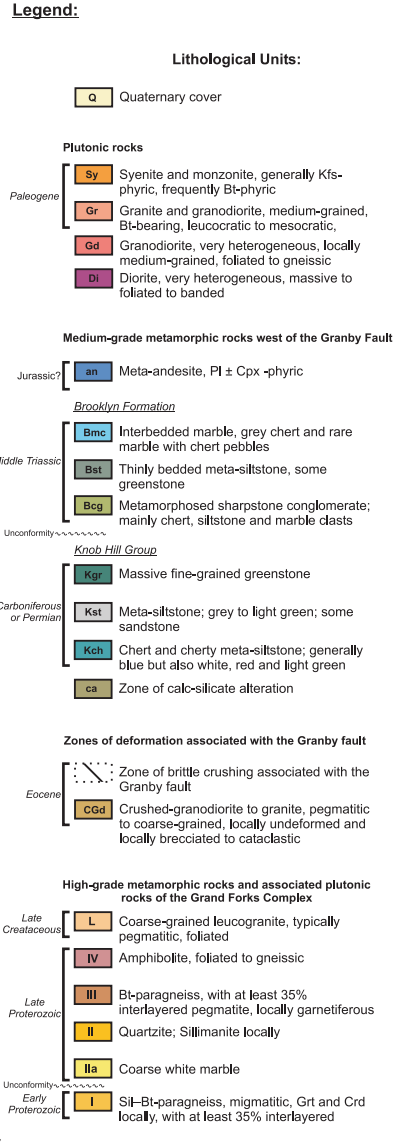
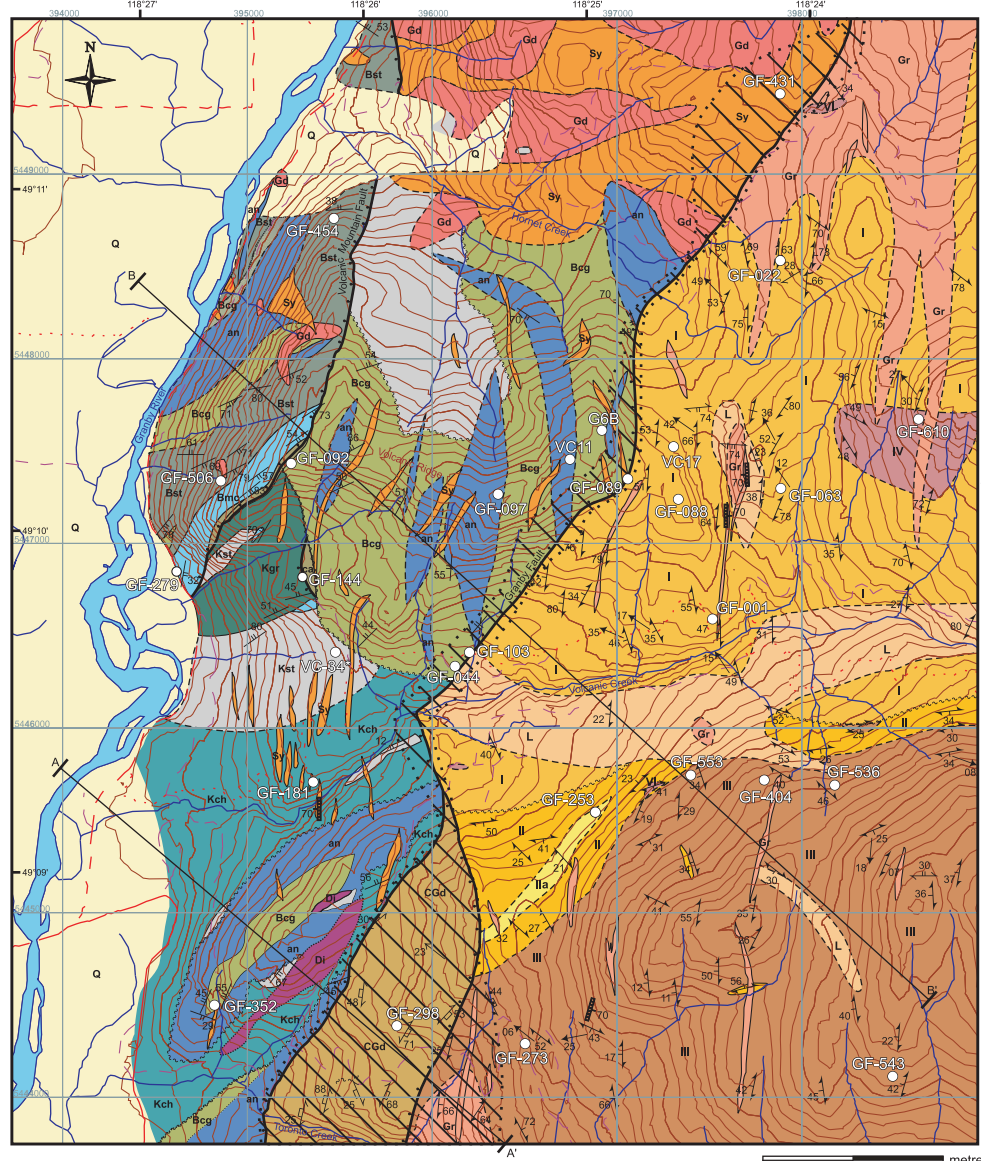
Fault zone

The zone of cataclasis and brecciation varies in thickness through the map area. In the central part, between Volcanic and Hornet Creek, the zone of brittle deformation is on aver-

age 100 m thick and affects both hanging-wall and footwall rocks. In the north, the crush zone is up to 230 thick and is largely restricted to the syenite unit (Sy) in the hanging wall. In the south, near Toronto Creek, the zone of brittle defor-

Fig. 2. Geological map of the Volcanic Creek area, southern British Columbia. 20 m contours, UTM Zone 11, NAD83. (a) Map; (b) cross-sections. (Laberge et al. 2004).

(a)



(b)

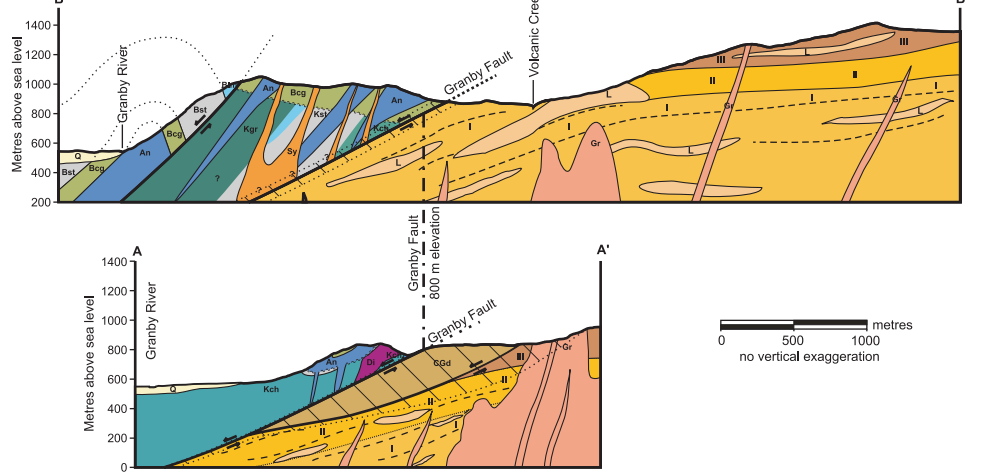
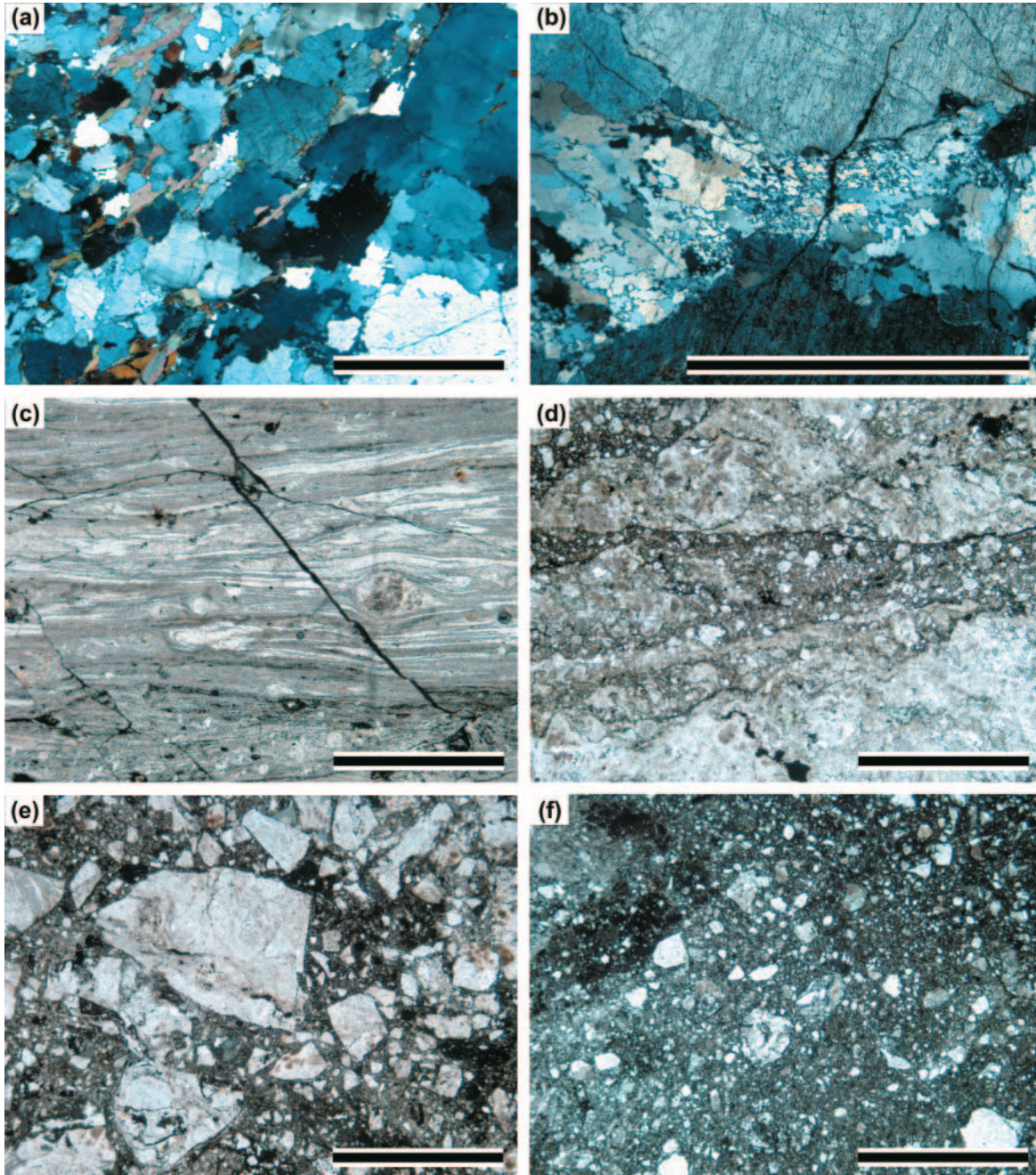


Table 1. Compilation of published isotopic dates in the vicinity of the Grand Forks complex.

Sample ID	NTS	Easting	Northing	Sample description	Age (Ma)	Reference
Grand Forks Complex - footwall of Granby Fault						
U–Pb zircon (detrital age)						
GF-1	82E/1	403860	5428406	Quartzite (GFC unit II)	650±15	Ross and Parrish 1991
GF-1A_B	82E/1	410720	5430386	calcareous paragneiss (GFC unit I)	(1681±1.5)	Armstrong et al. 1991
Rb–Sr whole rock						
GF-1 & 2 composite	82E/1	403860	5428406	GF-1: calcareous paragneiss; GF-2: paragneiss (GFC unit I)	(1695±794)	Armstrong et al. 1991
Sm–Nd whole rock						
GF-1 & 2 composite	82E/1	403860	5428406	GF-1: calcareous paragneiss; GF-2: paragneiss (GFC unit I)	(533±260)	Armstrong et al. 1991
K–Ar hornblende (cooling to ~530 °C)						
GSC 89-66	82E/1	393519	5434209	Hbl-syenite gneiss (GFC unit VIII of Preto 1969)	60±1	Hunt and Roddick 1990
GSC 80-50	82E/1	393461	5434341	Leucosyenite, foliated (GFC unit VIII of Preto 1970)	64.2±2.8	Stevens et al. 1982
K–Ar biotite (cooling to ~280 °C)						
GSC 80-49	82E/1	401516	5430319	garnetiferous granodiorite gneiss	49.1±2.5	Stevens et al. 1983
?	82E/1	396575	5443234	Pegmatite	51.7±3.6	Addie 1980
GSC 78-97	82E/1	399375	5441329	Pegmatite	50±2.4	Wanless et al. 1979
Hanging wall - of Granby Fault						
K–Ar whole rock (igneous cooling age?)						
ORO-128	82E/2	385250	5442531	Knob Hill schist	(150±10)	Church 1986
K–Ar biotite (cooling to ~280 °C)						
AK 112	82E/2	355769	5436362	Tuff? (Midway volcanic group)	50±4*	Mathews 1964
Late igneous intrusions						
U–Pb zircon (igneous crystallization age)						
Coryell Sy	82E/8	393980	5459964	coarse-grained syenite	51.1±0.5	Carr and Parkinson 1989
PCA-141-86	82E/8	409320	5480361	weak to moderately foliated biotite leucogranite	56±1	Parrish 1992
K–Ar biotite (cooling to ~280 °C)						
GSC 90-1	82E/7	386902	5480309	micaceous diorite	51.8±1.4	Hunt et al. 1991
GSC 90-3	82E/7	389819	5475183	Diorite	50.8±0.7	Hunt et al. 1991
GSC 90-2	82E/8	393609	5462752	Qtz-diorite	53.4±0.7	Hunt et al. 1991
GSC 66-46	82E/1	398707	5442101	Bt-qtz-monzonite, slightly deformed	48.5±3*	Wanless et al. 1968
GSC 66-45	82E/1	400391	5433564	undeformed granite	39.9±5*	Wanless et al. 1968
AK 25	82E/1	404865	5430113	Gneissic granite	(37±3.6*)	Baadsgaard et al. 1961
AK 28	82E/1	423195	5433535	Syenite	(56±5.4*)	Baadsgaard et al. 1961
GSC 60-20	82E/8	424340	5472436	Granite	(27.5±8*)	Lowdon 1961

Note: Data were compiled using the database of Breitsprecher and Mortensen (Breitsprecher and Mortensen 2004). Ages in parentheses have questionable analytical reliability as noted in their respective references. Ages with an asterisk* differ from published ages as they were recalibrated to more recent International Union of Geological Sciences (IUGS) constants (Steiger and Jäger 1977). National Topographic System (NTS) refers to the corresponding 1 : 50 000 map sheet. Universal Transverse Merator (UTM) coordinates are in Zone 11, referenced in the North American Datum (NAD)83. Hbl, hornblende.

Fig. 3. Photomicrographs showing the microstructures associated with the Granby fault. (a) Footwall: foliated, coarse-grained granite (GF-089.7), unaffected by the Granby fault (crossed-polarized light). (b) Footwall: foliated, coarse-grained granite (GF-088) ~200 m east of the fault. Note the evidence of strain in the subgrains in quartz (crossed-polarized light); (c) mylonitic texture in granodiorite GCd (GF-298B) with Kfs porphyroclasts and Qtz ribbons; (d) brecciated hanging-wall syenite (GF-431); (e) syenite breccia (GF-044). Angular to sub-angular fragments are consolidated breccias from early deformation; (f) cataclasite (GF-103), possibly crushed pegmatitic leucogranite. Scale bars = 2 mm.



mation is up to 300 m in thickness and is largely restricted to the crushed granodiorite unit (CGd) and some gneisses and pegmatite of the footwall.

Fault rocks

Fault zone rocks are cohesive breccias and cataclasites, recrystallized at moderate depths (Fig. 3). Brecciation is characterized by anastomosing cataclastic zones up to a few millimetres in thickness, containing fine- to coarse-grained

angular crushed crystals and rock fragments and secondary minerals, including epidote \pm chlorite \pm calcite, which cut through existing larger crystals (e.g., quartz and feldspars in pegmatite) or clasts in conglomerate. Brecciated fragments range from angular to subrounded. Fragments within the breccia commonly include slightly older consolidated fault breccia, which was already previously brittle deformed and recrystallized (Figs. 3d–3e), suggesting episodic movement along the fault. Cataclasites are fine-grained, green, and

Table 2. Mineral assemblages in selected samples from the footwall and hanging wall of the Granby fault.

Rock Type	Sample No.	Grt	Sil	Crd	Bt	Hbl	Act	Cpx	Ep	Kfs	Qtz	Pl	Spl	Ilm	Rt	Scp	Cal	Dol	Ol
Footwall																			
Paragneiss	GF-001	x	x	x ^a	x					x	x	x	x	x	x		x		
	GF-022	x	x	x ^a	x					x	x	x	x	x	x				
	GF-063		x	x ^a						x	x	x		x	x		x		
	GF-104	x	x	x	x					x	x	x		x					
	GF-372	x	x	x	x					x	x	x	x	x	x				
	GF-404				x					x	x	x						x	
	GF-536	x	x	x	x					x	x	x	x	x	x		x		
	GF-553	x			x					x	x	x						x	
Amphibolite	VC-17B				x	x					x	x							
	GF-273					x		x			x	x		x					
Marble	GF-253				x ^b								x				x	x	x
Hanging wall																			
Andesite	GF-097					x	x		x			x							x
	VC-11					x	x		x			x							x
Siltstone	VC-34	x			x				x		x	x		x	x				
	GF-144				x				x		x	x							
	GF-506				x	x					x	x		x	x				
Conglomerate	G6B				x	x					x	x		x					x
	GF-352					x		x	x		x	x			x				x
Skarn	GF-092	x						x	x		x			x	x	x			x
Limestone	VC-3				x						x								x

Note: Mineral abbreviations from Kretz (1983).

^aCompletely altered to sericite.

^bPhlogopite.

composed of recrystallized quartz and secondary epidote, chlorite, calcite, and fluorite, with remnant subrounded crystal fragments (usually quartz). No preferential fabric is developed, and microfaults or thin cataclastic zones do not follow any preferential orientation. Evidence for the late faulting occurs locally as far as 200 m east of the fault, where deformation is evidenced by subgrain development of quartz grains, while feldspars are unaffected (Fig. 3*b*). Closer to the fault, the deformation style is brittle, characterized by multiple brecciation events.

A medium- to very coarse-grained foliated to gneissic mesocratic granodiorite (unit CGd) occurs within the fault zone in the southern end of the map area, near Toronto Creek. The western margin of the unit, along the Granby fault, is characterized by brittle deformation similar to that observed elsewhere in the map area, with light green outcrops of fine-grained cataclasite occurring locally. The unit itself is locally brittly deformed, with occurrences of thin chloritized zones (1–10 mm thick) containing brecciated crystals. Discrete mylonitic fragments (Fig. 3*c*) also occur within this unit but lack lateral as well as longitudinal continuity, suggesting that they have been reworked by subsequent brittle deformation. The west-dipping, lens-shape intrusive body may have been intruded along the fault zone, early in the fault's history.

Petrology and mineral chemistry across the Granby fault

Grand Forks complex

Mineral assemblages from various rocks samples in the GFC (Fig. 2) are presented in Table 2. In this study, emphasis is placed on paragneiss, amphibolite, and marble.

Sillimanite-paragneiss

Migmatitic paragneiss contains the mineral assemblage Sil–Kfs–Pl–Qtz ± Crd ± Grt ± Ilm ± Spl ± Crn (abbreviations of Kretz 1983). All rocks contain trace amounts of apatite, rutile, monazite, and zircon as accessory phases. Banding is defined by alternating mesosomes and quartzo-feldspathic leucosomes, sometimes separated by thin, biotite-rich melanosomes (Fig. 4*a*). The mesosomes, typically 0.5–2 mm thick, are composed of sillimanite, cordierite, and ilmenite, with or without garnet, biotite, and spinel. Coarse-grained leucosomes, 1–20 mm thick, are composed of K-feldspar and quartz, with or without plagioclase, biotite, and rarely garnet or cordierite.

Quartz and feldspars constitute the dominant mineralogy of the paragneiss. K-feldspar, up to 30 modal percent, is most common in leucosomes as crystals up to 10 mm. Plagioclase occurs in mesosomes and leucosomes as small grains (<1 mm) representing 5% to 10% of the modal mineralogy. Sillimanite occurs as medium- to coarse-grained prismatic to acicular crystals. It is commonly associated with cordierite, ilmenite, and spinel in mesosomes (Fig. 4*b*). It rarely occurs within quartz or K-feldspar in leucosomes. Cordierite typically occurs in irregular anhedral form as elongated lenses or thin millimetre-scale bands with inclusions of one, or a combination, of sillimanite, garnet, ilmenite, spinel, and biotite (Fig. 4). Cordierite is also found as subhedral grains within leucosomes. It is usually completely altered to pinite.

Garnet is a rare phase in the paragneiss, but owing to its petrological significance, all samples described here are garnetiferous. In mesosomes, garnet porphyroblasts up to 5 mm in diameter are usually anhedral and rimmed by cordierite

Fig. 4. Photograph and photomicrographs of footwall paragneiss. (a) Migmatitic texture (GF-001, unit I); (b) garnet rimmed by altered cordierite (GF-022, unit I); (c) cordierite surrounding garnet (GF-372, unit I); (d) thin mesosome of prismatic sillimanite, ilmenite, and spinel in altered cordierite (GF-022, unit I); (e) large garnet porphyroblasts in cordierite mesosome (GF-536, unit III). Box marks location of (f). (f) Spinel-ilmenite in altered cordierite around the garnet porphyroblast in (e). Scale bar = 1 mm. Mineral abbreviations from Kretz (1983).

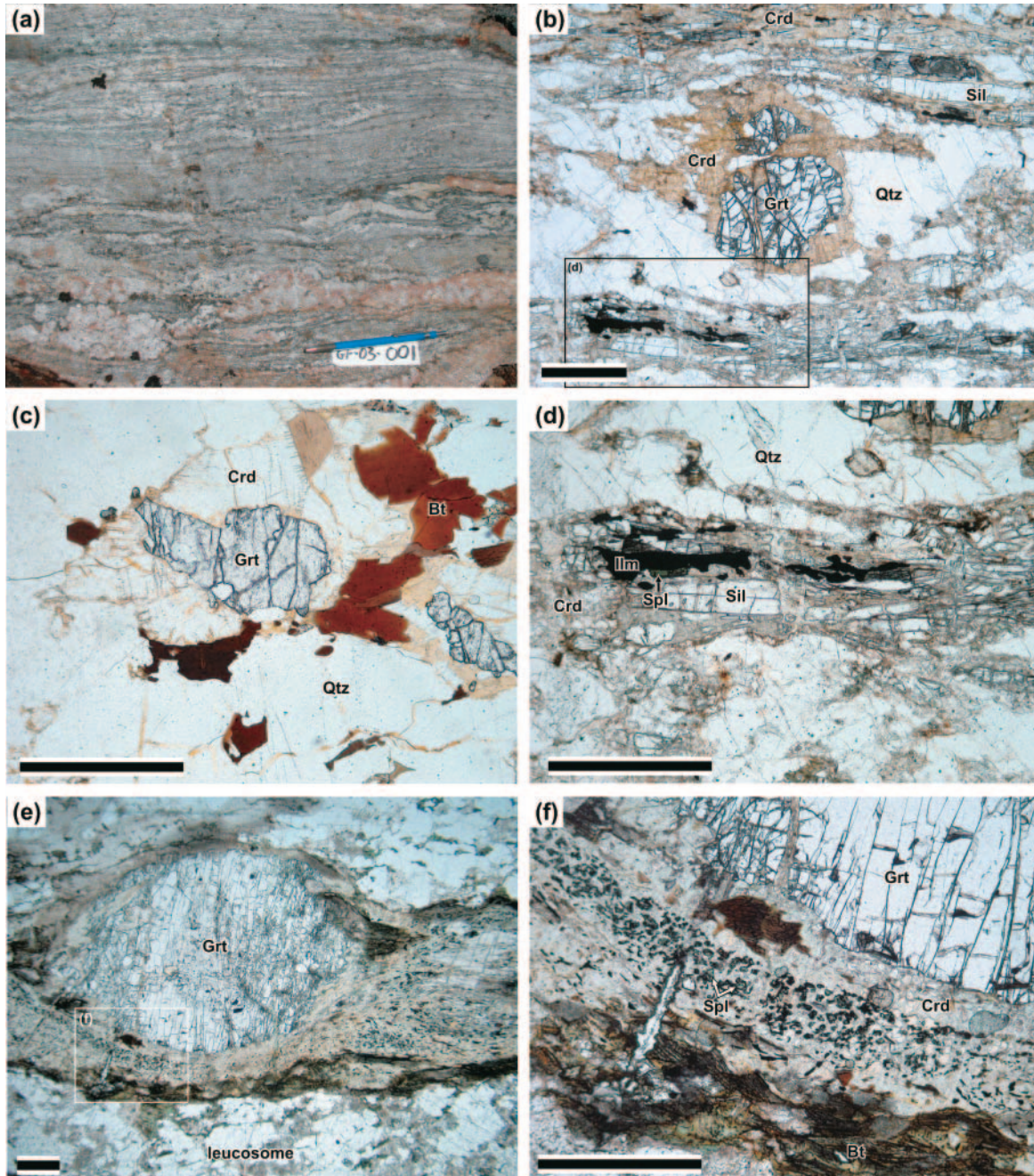


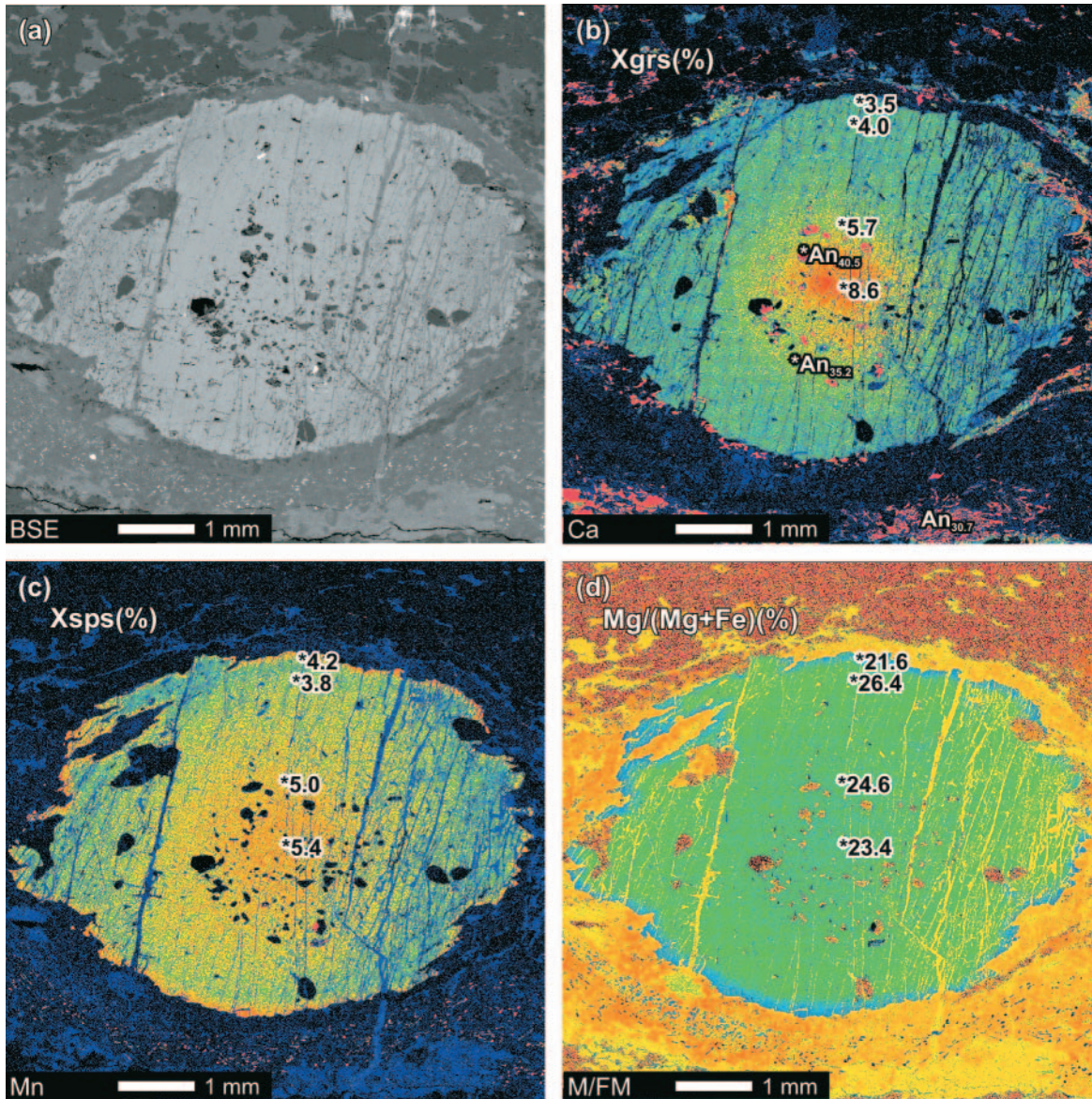
(Fig. 4), suggesting that some (but not all) of the cordierite in the rocks represents a product of garnet consumption. Garnet also occurs in leucosomes as discrete anhedral grains within quartz, where it is only locally rimmed by cordierite. The absence of cordierite rims on garnet seems to be associated with the absence of sillimanite in these bands.

Biotite occurs as subhedral laths typically 0.1 to 0.5 mm in size, mainly in mesosomes or melanosomes, but also in some leucosomes. The most biotite-rich horizons can have up to 20% biotite and are generally free of sillimanite and

cordierite. Biotite-poor horizons, with <~5% biotite, are sillimanite-rich and cordierite bearing. Ilmenite is present in small quantities (<<1%) in all samples. It occurs as fine anhedral grains <<0.5 mm, mainly as inclusions within the irregular cordierite masses.

Spinel is present in many samples in trace amounts, as very fine grains (<<0.2 mm). It always occurs as inclusions in cordierite, either associated with ilmenite in sillimanite-rich mesosome (Fig. 4d) or spatially associated with resorbed garnet (Fig. 4f). Fine-grained corundum occurs

Fig. 5. Compositional X-ray maps of a garnet crystal from Sil-paragneiss GF-536 for major divalent cations. Note remnant growth zoning in the Ca and Mn profiles and the thin Mn-enriched rim interpreted to be due to retrograde resorption. Proportions of end members were calculated from spot analyses at the specified locations. (a) Back-scattered electron image; (b) Ca-map with grossular content ($\text{Ca}/(\text{Ca} + \text{Fe} + \text{Mn} + \text{Mg})$); (c) Mn-map with spessartine content ($\text{Mn}/(\text{Ca} + \text{Fe} + \text{Mn} + \text{Mg})$); (d) $\text{Mg}/(\text{Mg} + \text{Fe})$ map. Maps were acquired with an acceleration voltage of 15.0 kV, beam current of 100 nA, dwell time of 20 ms, 1024 by 1024 points.



very locally, in trace amounts. It has only been observed in thin section from one locality. It is intergrown with fine-grained magnetite and is spatially associated with magnetite, ilmenite, and rarely with fine-grained spinel.

Three garnet-bearing gneiss samples have been studied in detail using electron microprobe analysis. GF-001 and GF-022 are samples from unit I, in which all observed cordierite is altered. Sample GF-536 is from unit III and contains altered cordierite, as well as some fresh cordierite inclusions in spinel. Garnet cores in GF-001 and GF-022 from unit I have $\text{Mg}/(\text{Mg} + \text{Fe})$ values of 0.12–0.16. In contrast, garnet cores in GF-536 from unit III have $\text{Mg}/(\text{Mg} + \text{Fe})$ values of 0.24–0.27. Resorption zoning is observed in all three samples as thin rims with lower $\text{Mg}/(\text{Mg} + \text{Fe})$ and grossular content, and higher Mn content (Fig. 5). These outer rims are inter-

preted to have developed from a retrograde net transfer reaction involving the consumption of garnet (Spear et al. 1999; Kohn and Spear 2000). Possible garnet consuming reactions are discussed later in the text.

Garnet growth zoning is generally not observed, consistent with expected reequilibration by diffusion at upper amphibolite- to granulite-facies conditions. An exception is a large garnet crystal in sample GF-536, which shows increasing concentrations of Fe, Mg, and $\text{Mg}/(\text{Fe} + \text{Mg})$ and decreasing concentrations of Mn and Ca, from the core to the rim (Fig. 5). This garnet crystal also has a resorbed outer rim, as previously described.

Biotite (magnesian annite) compositions are quite uniform within each sample, but vary between samples, with $\text{Mg}/(\text{Mg} + \text{Fe})$ ranging from 0.38 in GF-022 to 0.50 in the

leucosomes of GF-536. Ti content in biotite is variable within each sample, suggesting that some of the biotite could be retrograde. In GF-001 and GF-022, matrix plagioclase appears to have constant compositions averaging at An₃₃ and An₂₅, respectively, (Table 3). In GF-536, matrix plagioclase has a composition of An₃₁. Plagioclase inclusions within garnet in GF-536 are more calcic than matrix plagioclase, reaching An₄₀ close to the garnet core.

Unaltered cordierite has only been observed in sample GF-536, where it occurs as small inclusions within spinel crystals. The cordierite inclusions have Mg/(Fe + Mg) ratios between 0.61 and 0.65. Spinel is Fe-rich with hercynite content commonly around 80%, but ranging from 60% to 88%. Locally, gahnite (Zn end member) can represent up to 25% of the composition (in GF-001), but is more commonly between 1% to 5%.

Biotite-parageniss

Biotite-parageniss, typically migmatitic, is widespread and may be interlayered with the sillimanite-paragneiss (Fig. 6e). It is characterized by the assemblage Kfs–Pl–Qtz–Bt ± Grt (Fig. 6f), in addition to quartzofeldspathic leucosomes a few millimetres to centimetres thick.

Amphibolite

The amphibolite has a coarse-grained, foliated to gneissic texture (Fig. 6a). Alternating amphibole-rich and leucocratic bands are usually 1–4 mm thick. The mineral assemblage is Hbl–Pl–Ilm–Mag–Ttn ± Cpx ± Bt. Clinopyroxene (Cpx)-free amphibolite, the most common variety, is weakly foliated and displays rare millimetre-thick leucocratic bands of plagioclase and quartz, which locally give the rocks a migmatitic appearance. Clinopyroxene-bearing amphibolite is foliated and compositionally banded. Dark hornblende-rich layers with some plagioclase and clinopyroxene alternate with light-coloured layers containing mainly plagioclase and clinopyroxene (Fig. 6b). The composition of the hornblende, clinopyroxene, and biotite is uniform at the thin-section scale, and no zoning is observed. In VC-17B, Mg/(Fe + Mg) in pargasitic hornblende and biotite is 0.57 and 0.56, respectively, (Table 4). In GF-273, Mg/(Fe + Mg) in pargasitic hornblende, clinopyroxene, and biotite are 0.52, 0.68, and 0.51, respectively. Plagioclase is labradorite with variable anorthite content of An_{50–56} in Cpx-bearing sample GF-273 and An_{60–70} in Cpx-free sample VC-17B.

Marble

The marble mainly consists of coarse-grained calcite and dolomite crystals 1–3 mm in size. Compositional banding is common with 5–30 mm thick layers of coarse calcite and dolomite alternating with 5–10 mm thick layers enriched in accessory minerals including olivine, diopside, spinel, and phlogopite (Fig. 6c). Accessory minerals typically form <5 modal percent of the marble. Magnesian olivine (Fo₉₇) occurs as subhedral to anhedral crystals ≤1 mm in diameter (Fig. 6d). Magnesian spinel (X_{Mg} = 87%–90%) occurs as euhedral to subhedral crystals <1 mm in diameter and shows compositional zoning, with slight decrease in Mg content and increase in Ti content towards the rim. Phlogopite occurs as subhedral laths <1 mm in length and has a Mg/(Fe + Mg) ratio of 0.97 (Table 4).

Hanging wall of the Granby fault

The supracrustal rocks exposed west of the Granby fault in the field area include metamorphosed chert, siltstone, sandstone, polymictic sharpstone–conglomerate, skarn, limestone, and porphyritic andesite (Laberge et al. 2004; Laberge 2005) (Fig. 2). Representative mineral assemblages are presented in Table 2. For the purpose of phase equilibria, only samples of metasiltstone from the Knob Hill Group and meta-andesite will be discussed further.

Calcic metasiltstone

The fine-grained calcic metasiltstone sample VC-34 is characterized by the mineral assemblage Grt–Ep–Bt–Pl–Qtz–Rt–Ilm–Mag (Figs. 7a, 7b). Idiomorphic garnet porphyroblasts are ≤100 μm in diameter, locally hosting fine quartz and epidote inclusions. Matrix minerals have an average grain size of ~10 μm, with subhedral biotite and anhedral quartz and plagioclase. Garnet is manganiferous and displays weak concentric growth zoning, with a small decrease in Mn and increase in Fe from core to rim, from 47% to 42% in spessartine content, and 38% to 43% in almandine content (Fig. 8). Calcium content does not vary significantly from core to rim. Biotite, which is idiomorphic, has a homogeneous composition with a mean Mg/(Fe + Mg) ratio of 0.61 (Table 5). The composition of epidote is quite variable with the Fe³⁺ end member (epidote) ranging from 64% to 84%, while the Mn end member (piemontite) ranges from 10% to 4%. The spatial relationship between the two varieties is not well understood. Plagioclase crystals generally have calcic cores (~An₅₂) and sodic rims (~An₃₀) (Table 5).

Meta-andesite

Meta-andesite is fine-grained and generally porphyritic, containing small (<2 mm) plagioclase phenocrysts and locally large (2–6 mm) amphibole pseudomorphs after clinopyroxene phenocrysts (Fig. 7c). Plagioclase laths of igneous texture but metamorphic composition are preserved in the matrix, along with metamorphic actinolite, hornblende, epidote, calcite and minor quartz. Magnesiohornblende and actinolite are complexly intergrown in the relict phenocrysts. Magnesiohornblende typically occurs near the core of the relict clinopyroxene phenocrysts, while actinolite occurs as an irregular network of bands within and around hornblende (Figs. 7d, 9). They have significantly different Al–Si content, as well as different Mg/(Fe + Mg) ratios, with actinolite slightly more magnesian than hornblende. Matrix amphiboles in GF-097 are magnesiohornblende with clustered compositions, while matrix amphiboles in VC-11 range in composition from actinolite to magnesiohornblende.

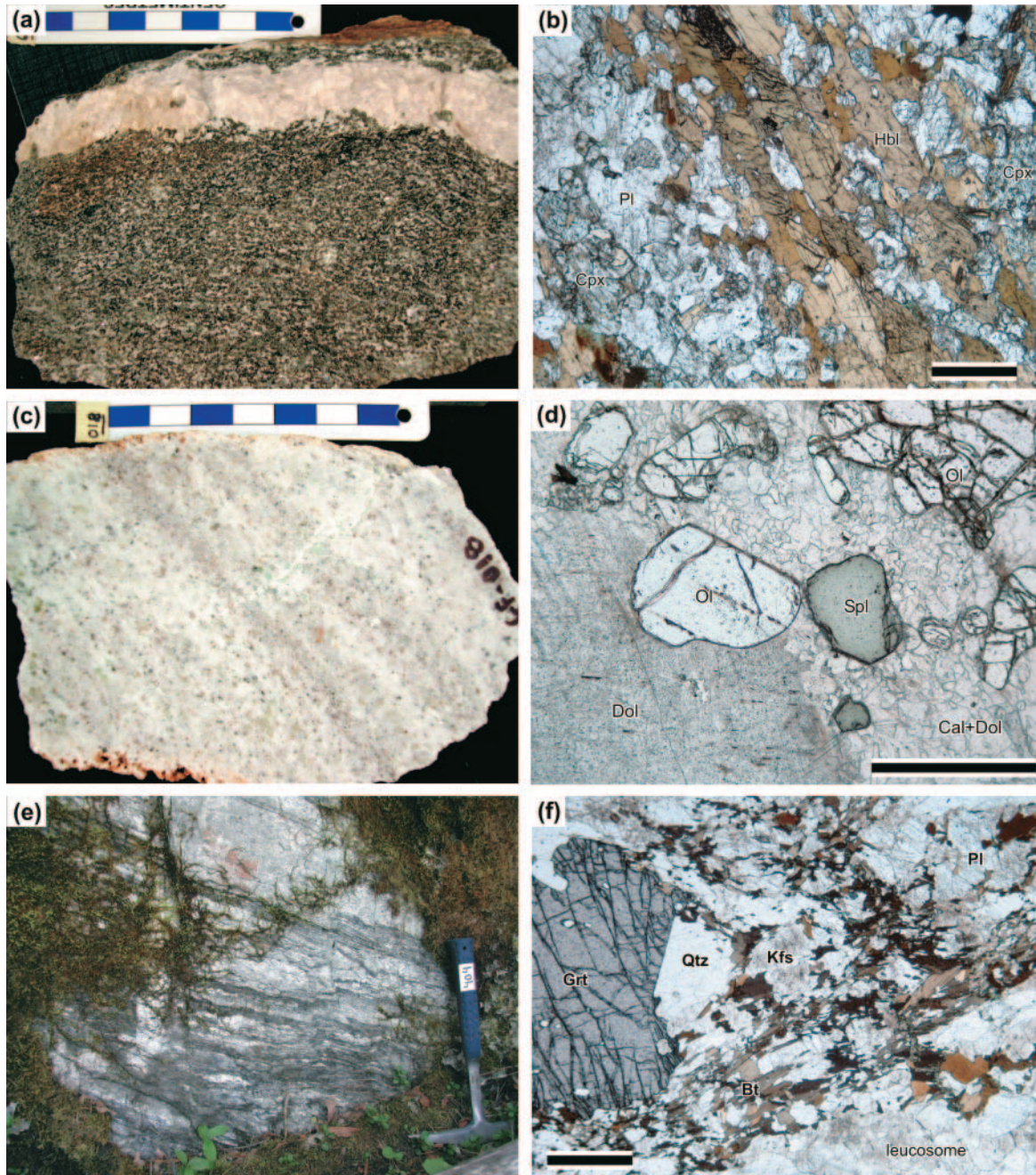
Plagioclase crystals are compositionally zoned, with labradorite cores (An₆₈) and oligoclase rims (An₂₉), as in sample GF-097. The rims are interpreted to represent metamorphic plagioclase surrounding relict igneous cores. No clear zoning pattern is observed in sample VC-11, but plagioclase composition varies only from An₂₉ to An₄₀. Epidote is an accessory phase occurring within the relict phenocrysts and the matrix. Chemical analyses show a high mole fraction of the epidote versus the clinozoisite end member with X_{Ep} = 0.93.

Table 3. Representative mineral compositions in paragneiss from the GFC.

Rock:	Sillimanite-paragneiss																	
Mineral:	Garnet							Biotite				Cordierite	Plagioclase			Spinel		
Sample:	GF-001		GF-022		GF-536			GF-001	GF-022	GF-536		GF-536	GF-001	GF022	GF-536	GF-001	GF-022	GF-536
Note:	core	rim	core	rim	core	rim	outer rim	matrix	matrix	matrix	leuco-some		matrix	matrix	matrix	matrix	matrix	grt rim
Oxides (wt.%)																		
SiO ₂	37.01	37.66	37.40	37.13	37.53	37.78	37.13	35.83	35.08	34.66	35.87	47.81	59.69	62.06	60.58			
TiO ₂								4.56	3.04	5.27	4.66					0.00	0.04	0.04
Al ₂ O ₃	20.95	20.78	20.76	20.69	20.67	20.87	20.57	17.36	18.28	17.60	15.69	33.37	25.83	24.48	25.42	55.96	58.87	58.81
Cr ₂ O ₃																0.15	0.07	0.11
FeO	28.58	28.78	36.40	37.58	31.34	32.32	34.85	20.49	21.79	20.34	18.93	8.14	0.05	0.08	0.18	37.72	37.11	34.97
MnO	7.72	9.04	1.17	1.37	2.53	1.82	2.56	0.22	0.11	0.11	0.09	0.19				0.89	0.27	0.33
MgO	2.91	2.24	3.80	2.72	5.37	6.43	4.06	8.71	7.61	8.15	10.44	7.60				4.10	2.87	4.57
ZnO																0.97	2.32	0.78
CaO	2.35	2.13	1.12	0.83	3.18	1.44	1.31	0.01	0.02	0.00	0.02	0.01	6.97	5.04	6.24			
Na ₂ O								0.22	0.23	0.21	0.33	0.67	7.35	8.18	7.52			
K ₂ O								9.51	9.86	9.77	9.95	0.02	0.35	0.42	0.39			
F								0.37	0.06	0.20	0.44							
Total	99.51	100.63	100.65	100.31	100.71	100.67	100.51	97.27	96.07	96.30	96.40	97.80	100.24	100.24	100.30	99.79	101.56	99.60
Cations																		
Si	2.994	3.024	2.996	3.003	2.973	2.979	2.982	2.703	2.694	2.647	2.728	4.962	2.654	2.742	2.686	0.000	0.001	0.001
Ti								0.259	0.176	0.303	0.266					1.881	1.950	1.955
Al	1.998	1.968	1.961	1.973	1.930	1.940	1.947	1.544	1.655	1.584	1.407	4.083	1.354	1.275	1.329			
Fe	1.933	1.933	2.439	2.542	2.076	2.132	2.341	1.293	1.399	1.299	1.204	0.706	0.002	0.002	0.006	0.900	0.872	0.825
Mn	0.529	0.615	0.079	0.093	0.170	0.122	0.174	0.014	0.007	0.007	0.006	0.017				0.022	0.006	0.008
Mg	0.350	0.269	0.454	0.328	0.634	0.756	0.486	0.979	0.870	0.927	1.183	1.131				0.174	0.120	0.192
Zn																0.020	0.048	0.016
Ca	0.203	0.183	0.096	0.072	0.270	0.121	0.113					0.001	0.332	0.239	0.296			
Na								0.032	0.034	0.031	0.048	0.105	0.634	0.701	0.647			
K								0.915	0.966	0.952	0.965	0.003	0.020	0.024	0.022			
Sum	8.008	7.992	8.024	8.011	8.057	8.050	8.044	7.740	7.803	7.749	7.809	11.006	4.996	4.983	4.984	3.000	3.000	0.000
M/FM	0.153	0.122	0.157	0.114	0.234	0.262	0.172	0.431	0.383	0.416	0.496	0.616				0.182	0.127	0.197
xAb													0.643	0.728	0.670			
xAn													0.337	0.248	0.307			
xOr													0.020	0.025	0.023			

Note: All Fe assumed to be ferrous. The number of cations is based on structural formulae with 12, 11, 18, 8, and 4 oxygens for garnet, biotite, cordierite, plagioclase, and spinel, respectively. M/FM = Mg/(Mg + Fe); xAb = Na/(Na + Ca + K); xAn = Ca/(Na + Ca + K); xOr = K/(Na + Ca + K).

Fig. 6. Photographs and photomicrographs of footwall rocks. (a) Weakly foliated amphibolite with quartzofeldspathic vein (GF-610, unit IV). (b) Compositional layering in a Cpx-bearing amphibolite (GF-273, unit IV). (c) Compositional layering in marble (GF-018, unit II) defined by bands enriched in olivine and spinel. (d) Subhedral spinel and olivine in calcite-dolomite marble (GF-253, unit II). (e) Stromatic biotite-paragneiss showing lens-shaped quartz-rich leucosome in the lower biotite-rich horizon, and a thin quartzite band in the upper portion (GF-404, unit III). (f) Garnet porphyroblasts in a biotite-rich mesosome in Grt–Bt-paragneiss (GF-553, unit III). Scale bars are in centimetres for hand sample photographs and are 1 mm long in photomicrographs. Mineral abbreviations from Kretz (1983).



High-grade metamorphism of the GFC

The presence of sillimanite, garnet, cordierite, and K-feldspar in the footwall paragneiss, combined with the absence of orthopyroxene and garnet in the amphibolite, indicates that the complex is in the transitional zone between upper amphibolite and granulite facies at low–moderate pressure. Peak P – T conditions are, therefore, in the range

of 5–8 kbar (1 kbar = 100 MPa), 750–850 °C (Pattison et al. 2003).

Methodology

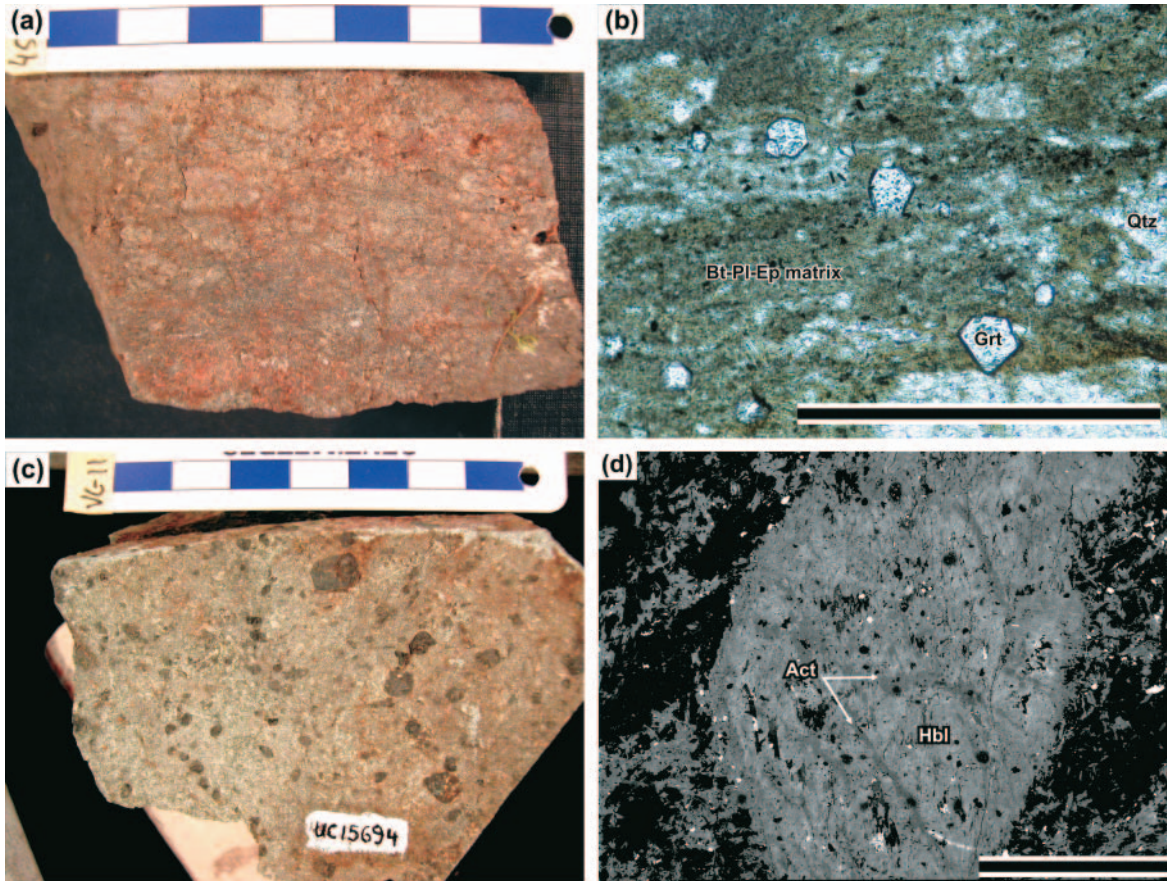
P – T conditions during metamorphism were estimated more precisely using a combination of phase equilibria constraints and thermobarometry. For thermobarometry, calibrations of individual T -sensitive exchange equilibria (Table 6) and a

Table 4. Representative mineral compositions in amphibolite and marble from the GFC.

Rock:	Amphibolite						Marble						
Mineral:	Amphibole		Diopside	Biotite		Plagioclase		Olivine	Spinel		Biotite	Calcite	Dolomite
Sample:	GF-273	VC-17B	GF-273	GF-273	VC-17B	GF-273	VC-17B	GF-253	GF-253	GF-253	GF-253	GF-253	GF-253
Oxides (wt.%)									core	rim			
SiO ₂	41.48	42.64	52.83	35.47	37.65	55.26	51.84	42.34			39.21		
TiO ₂	3.13	2.37	0.06	4.48	4.77				0.06	0.28	0.91		
Al ₂ O ₃	12.35	11.53	0.43	14.63	14.52	28.97	30.70		67.14	66.00	16.33		
FeO	16.21	15.43	10.44	19.65	17.57	0.11	0.24	2.45	5.22	6.87	1.33	0.09	0.38
MnO	0.20	0.31	0.31	0.14	0.20			0.07	0.00	0.00	0.03	0.06	0.05
MgO	9.72	11.68	12.35	11.31	12.78			55.44	27.07	26.41	26.84	2.15	20.94
CaO	11.72	11.95	23.93	0.03	0.02	10.82	13.24				0.07	53.57	30.97
Na ₂ O	1.92	1.39	0.17	0.21	0.15	5.26	3.92				0.48		
K ₂ O	—	1.59		9.92	9.47	0.25	0.14				9.80		
F				0.24	0.49						0.53		
CO ₂												44.48	47.42
Total	96.74	98.90	100.51	96.07	97.62	100.66	100.08	100.30	99.490	99.550	95.54	100.35	99.75
Cations													
Si	6.234	6.329	1.985	2.718	2.794	2.474	2.353	1.000			2.755		
Ti	0.354	0.264	0.002	0.258	0.266				0.001	0.005	0.048		
Al	2.187	2.016	0.019	1.322	1.270	1.529	1.643		1.912	1.892	1.352		
Fe	2.038	1.915	0.328	1.260	1.090	0.004	0.009	0.048	0.105	0.140	0.078	0.001	0.005
Mn	0.026	0.039	0.010	0.009	0.012			0.001	0.000	0.000	0.001	0.001	0.001
Mg	2.177	2.584	0.691	1.292	1.413			1.951	0.975	0.958	2.810	0.053	0.482
Ca	1.888	1.900	0.963			0.519	0.644					0.945	0.513
Na	0.463	0.400	0.012	0.030	0.021	0.456	0.345				0.065		
K	0.368	0.301		0.970	0.896	0.014	0.008				0.878		
Sum	15.734	15.749	4.010	7.863	7.765	4.997	5.002	3.000	3.000	3.000	7.993	1.000	1.000
M/FM	0.516	0.574	0.678	0.506	0.564			0.976	0.979	0.957	0.973		
xAb						0.461	0.346						
xAn						0.525	0.646						
xOr						0.015	0.008						

Note: All Fe assumed to be ferrous. The number of cations is based on structural formulae with 23, 6, 11, 8, 4, and 4 oxygen equivalents for amphibole, diopside, biotite, plagioclase, olivine and spinel and, respectively. M/FM = Mg/(Mg + Fe), xAb = Na/(Na + Ca + K); xAn = Ca/(Na + Ca + K); xOr = K/(Na + Ca + K).

Fig. 7. Hanging-wall rocks. (a) Reddish-weathered, grey siltstone (GF-454, unit Bst). Scale bar in centimetres. (b) Garnet porphyroblasts in a very fine-grained Bt–Ep–Pl–Qtz matrix in siltstone (VC-34, unit Kst). Scale bar = 1 mm. (c) Porphyritic texture in meta-andesite (VC-11, unit an). Scale bar in centimetres. (d) backscattered-electron image of amphibole pseudomorphs after clinopyroxene phenocrysts in andesite, showing an irregular network of actinolite bands in hornblende (VC-11, unit an). Mineral abbreviations from Kretz (1983).



multi-equilibrium statistical approach (Table 7) were applied. The multi-equilibrium estimates were calculated with the internally consistent thermodynamic data of Holland and Powell (1998; 2002 update) using THERMOCALC 3.21. End-member activities were calculated using the AX program of Tim Holland (2000 version).

Because the electron microprobe does not permit direct measurement of H₂O content in minerals, the activity of H₂O in cordierite was constrained qualitatively. In many granulite terranes, cordierite has relatively low H₂O contents between 0.6 and 1.2 wt.%, and H₂O activities are also generally low, between 0.1 and 0.4 (Harley et al. 2002). Therefore, *P–T* calculations were performed within this range of water activity, and the best statistical fit of the data was obtained with a water activity of 0.2.

Phase equilibria: A petrogenetic grid in KFMASH for metapelites

Many mineral reactions affecting high-grade metapelitic rocks can be modeled satisfactorily in the simplified chemical system K₂O–FeO–MgO–Al₂O₃–SiO₂–H₂O (KFMASH). A petrogenetic grid for high-grade, supersolidus metapelites is presented in Fig. 10a. Phase equilibria were calculated using THERMOCALC (Powell and Holland) and the thermodynamic data of Holland and Powell (1998; 2002 update).

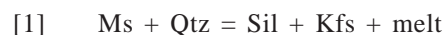
Phases considered are Grt–Bt–Crd–Opx–Spl–Sil–Qtz–Kfs–melt. Melting reactions assume no free H₂O; all the water derived from hydrous phases is dissolved into the melt fraction. K-feldspar and melt are assumed to be in excess. Mixing models follow White et al. (2001).

In the KFMASH grid, reaction coefficients vary along reaction curves, reflecting the change in composition of phases with pressure and temperature. Continuous reactions that are divariant with respect to Fe/(Fe + Mg) may be represented by isopleths of fixed Fe/(Fe + Mg). In Fig. 10b, isopleths of Fe/(Fe + Mg) in garnet are shown.

Peak assemblage: Grt–Pl–Bt–Qtz ± Sil ± Crd

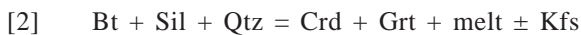
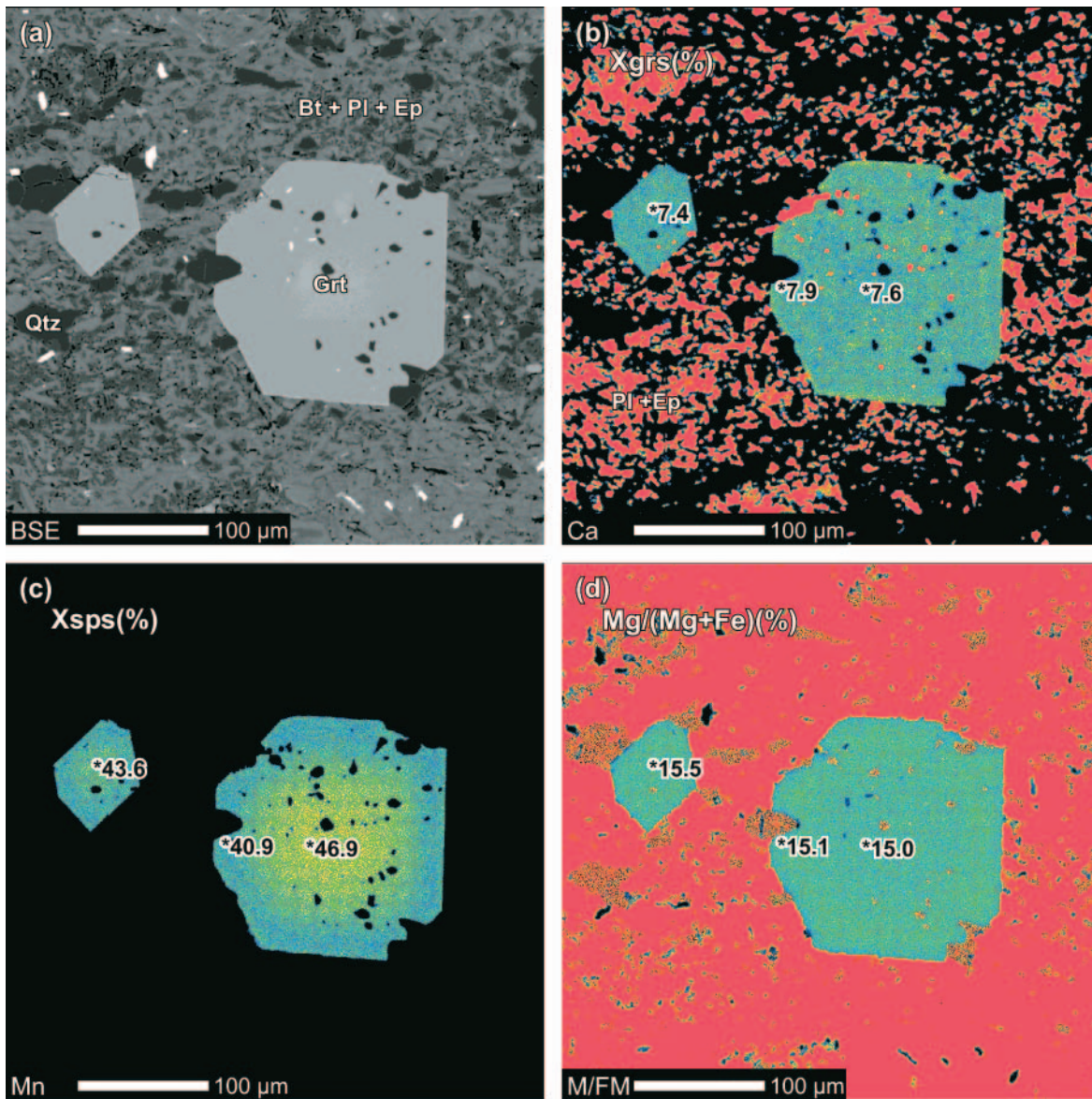
The mineral assemblage interpreted as representing peak metamorphic conditions in the high-grade metapelites consists of Sil–Crd–Bt–Kfs–Qtz–Pl–melt ± Grt. *P–T* conditions can be inferred from Fig. 10a as follows.

The absence of prograde muscovite indicates that the peak temperature is above the muscovite breakdown melting reaction.



The stability of garnet and cordierite indicates that *P–T* conditions reached the biotite + sillimanite melting reaction

Fig. 8. Compositional X-ray maps of a garnet porphyroblast in metasilstone VC-34, for major divalent cations. Proportions of end members were calculated from spot analyses at specified locations. (a) Back-scattered electron image; (b) Ca-map with grossular content (Ca/(Ca + Fe + Mn + Mg)); (c) Mn-map with spessartine content (Mn/(Ca + Fe + Mn + Mg)); (d) Mg/(Mg + Fe) map. Maps were acquired with an acceleration voltage of 15.0 kV, beam current of 100 nA, dwell time of 20 ms, 1024 by 1024 points. Mineral abbreviations from Kretz (1983).



The absence of orthopyroxene in sillimanite-free garnet-biotite paragneiss suggests that peak temperatures are below the reaction



Reaction [2] is of most significance to the observed peak assemblage. Since all phases involved as products and reactants are present as major minerals in the assemblage, it is likely that *P-T* conditions did not markedly exceed this reaction, recognizing that the presence of Ti, F, and other minor elements in biotite renders reaction [2] multivariant and that some of the biotite in the rocks appears to be retrograde (see earlier in the text). The divariant field bounded by reaction 2

and 3 (Fig. 10a), therefore, represents the *P-T* domain of peak metamorphic conditions.

Measured values of Fe/(Fe + Mg) from the compositional “central plateau” regions of garnet, excluding data from the retrograde rims, are used to further bracket peak *P-T* conditions (Fig. 10b). Isopleths corresponding to these values lead to a peak *P-T* estimate of 800 ± 35 °C and 5.8 ± 0.6 kbar.

Late assemblage *Grt-Crd-Spl-Sil ± Qtz*

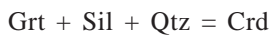
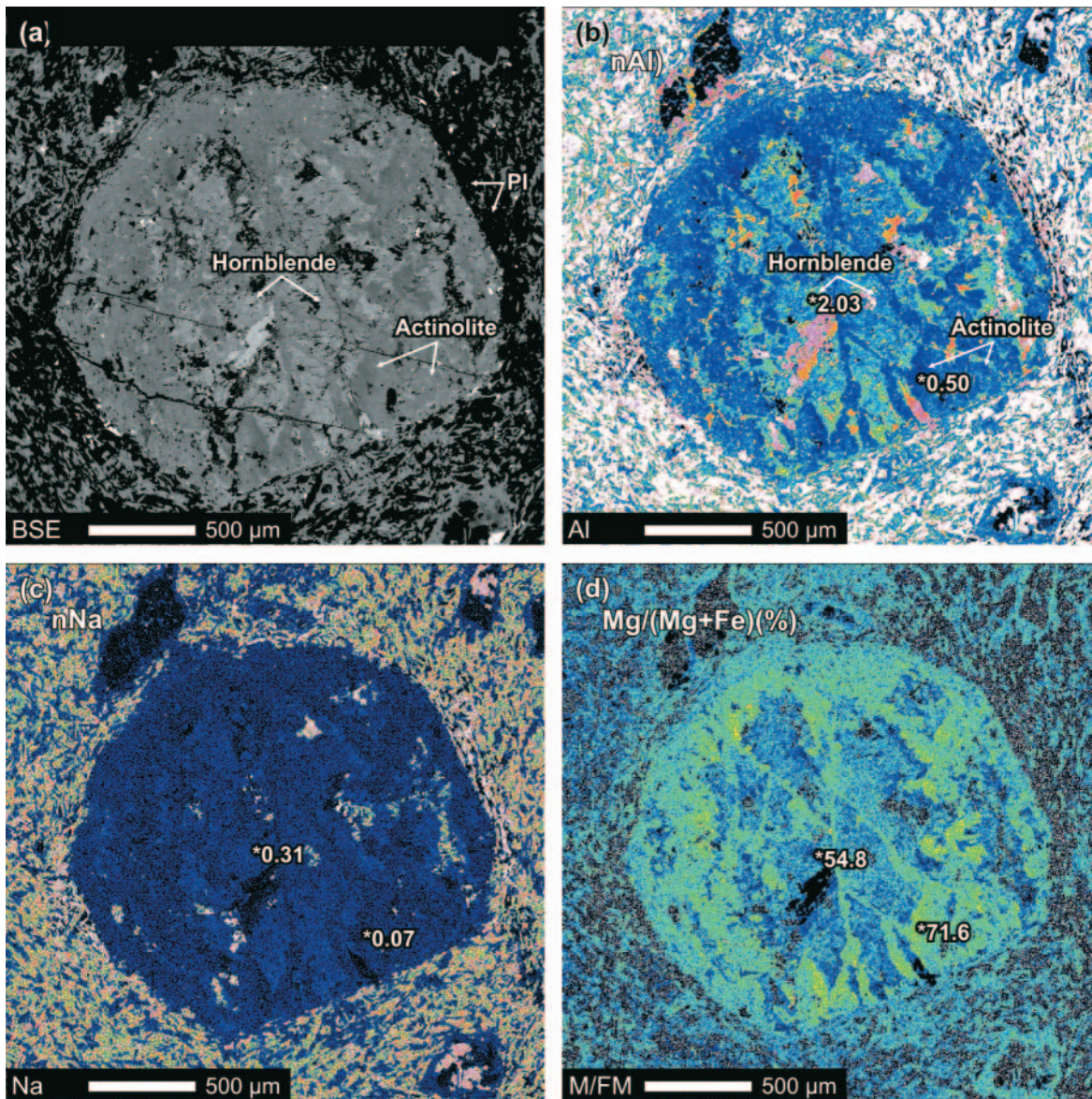
Garnet typically has textures indicative of resorption in the Sil-paragneiss, with the exception of some garnet in leucosome. Cordierite coronas around garnet in the presence of sillimanite are common, suggesting that garnet resorption leading to cordierite growth resulted from the net-transfer reaction

Table 5. Representative mineral compositions in metasiltstone and meta-andesite samples from the hangingwall of the Granby fault.

Rock:	Metasiltstone							Meta-andesite										
Mineral:	Garnet		Biotite	Plagioclase		Epidote			Amphibole						Plagioclase		Epidote	
Sample:	VC-34							GF-097			VC-11				GF-097		VC-11	GF097
Note:	core	rim		rim	core	core	rim	pheno Act	pheno Hbl	matrix Hbl	pheno Act	pheno Hbl	matrix Act	matrix Hbl	matrix core	matrix rim		
Oxides (wt.%)																		
SiO ₂	36.87	37.27	35.76	60.41	55.03	37.32	37.47	52.28	44.15	49.90	50.79	47.27	51.88	48.37	53.04	59.73	60.61	37.44
TiO ₂			1.34			0.06	0.09	0.06	0.22	0.22	0.07	0.28	0.25	0.21				0.02
Al ₂ O ₃	20.34	20.65	16.79	25.03	28.82	24.49	22.56	2.92	11.58	5.60	4.50	8.14	3.45	6.06	29.93	24.78	25.64	22.34
FeO	17.13	19.37	16.28	0.11	0.33	11.36	13.41	11.62	16.38	14.68	13.53	15.84	13.04	14.73	0.21	0.13	0.20	14.10
MnO	20.58	18.38	0.36			1.50	0.65	0.42	0.42	0.42	0.52	0.53	0.56	0.50				0.11
MgO	1.71	1.90	14.30			0.08	0.06	16.49	11.13	14.10	14.51	12.12	15.22	14.47				0.10
CaO	2.77	2.69	0.04	6.09	10.57	21.85	22.65	12.76	12.34	12.58	12.36	12.07	12.25	11.51	11.61	5.93	6.11	23.72
Na ₂ O			0.15	7.85	5.38	0.03	0.03	0.28	1.17	0.54	0.42	0.97	0.44	0.52	4.49	7.64	8.10	0.01
K ₂ O			9.13	0.09	0.15	0.06	0.03	0.09	0.31	0.23	0.16	0.27	0.08	0.16	0.14	0.38	0.17	0.03
F			0.12								0.00	0.00	0.02	0.00				
Cl																		
SO ₃																		
Total	99.40	100.25	98.10	99.59	100.28	98.00	98.45	96.91	97.70	98.28	96.85	97.49	97.17	96.50	99.41	98.59	100.83	99.45
Cations																		
Si	3.010	3.011	2.723	2.694	2.474	2.966	2.987	7.588	6.581	7.271	7.452	7.008	7.557	7.178	2.410	2.694	2.675	2.957
Ti	0.000	0.000	0.077			0.003	0.005	0.007	0.024	0.024	0.007	0.031	0.028	0.023				0.001
Al	1.957	1.967	1.507	1.316	1.528	2.294	2.119	0.500	2.036	0.962	0.778	1.422	0.592	1.060	1.603	1.317	1.334	2.079
Fe ²⁺	1.170	1.309	1.037	0.004	0.012	0.119	0.050	1.411	2.042	1.790	1.660	1.964	1.589	1.828	0.008	0.005	0.007	0.000
Fe ³⁺						0.636	0.844											0.931
Mn	1.423	1.258	0.023			0.101	0.044	0.051	0.053	0.052	0.065	0.067	0.069	0.062				0.007
Mg	0.208	0.229	1.623			0.009	0.007	3.567	2.471	3.062	3.172	2.677	3.303	3.200				0.012
Ca	0.243	0.233		0.291	0.509	1.860	1.935	1.985	1.971	1.964	1.943	1.918	1.912	1.829	0.565	0.287	0.289	2.007
Na			0.022	0.679	0.469	0.005	0.005	0.078	0.338	0.153	0.121	0.280	0.124	0.148	0.396	0.668	0.693	0.002
K			0.887	0.005	0.008	0.006	0.004	0.017	0.059	0.043	0.030	0.050	0.014	0.030	0.008	0.022	0.009	0.003
Sum	8.011	8.006	7.902	4.990	5.001	8.000	8.000	15.204	15.575	15.322	15.227	15.416	15.188	15.358	4.990	4.993	5.009	8.000
M/FM	0.151	0.149	0.610					0.716	0.548	0.631	0.656	0.577	0.675	0.636				
xAb				0.696	0.476										0.409	0.684	0.699	
xAn				0.299	0.516										0.583	0.294	0.292	
xOr				0.005	0.008										0.008	0.022	0.009	

Note: Mineral abbreviations from Kretz (1983). The number of cations is based on structural formulae with 12, 11, 8, 13, and 23 oxygen equivalents for garnet, biotite, plagioclase, epidote, and amphibole, respectively. Estimations of Fe³⁺ in epidote assumes that (Si + Al + Ti + Fe³⁺ + Mn³⁺) ≤ 6 (normalized on 8 cations). In other minerals, all Fe is assumed to be ferrous. M/FM = Mg/(Mg + Fe); xAb = Na/(Na + Ca + K); xAn = Ca/(Na + Ca + K); xOr = K/(Na + Ca + K).

Fig. 9. Composition X-ray maps of amphiboles within a relict phenocryst in meta-andesite GF-097, showing a hornblende core, complex rim, and network of actinolite. (a) back-scattered electron image; (b) Al-map; (c) Na-map; (d) Mg/(Mg + Fe) map. *n*Al and *n*Na are the number of cations per formula unit. Values shown in the core and rim are averages of several analyses of hornblende and actinolite in the pseudomorph. Maps were acquired with an acceleration voltage of 15.0 kV, beam current of 20 nA, dwell time of 25 ms, 1024 by 1024 points.



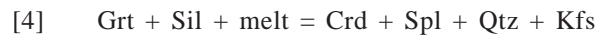
This reaction corresponds to the biotite-free Fe/(Fe + Mg) isopleths between reaction [2] and [4] in Fig. 10b. In *P-T* space, its slope is very shallow ($dP/dT \approx 0$) so that at least some component of decompression is required to cross the reaction.

Spinel is locally observed in cordierite within coronas around resorbed garnet. Cordierite and spinel are inferred to have crystallized from the garnet-consuming decompression reaction



In the full KFMASH system, this reaction additionally involves minor amounts of K-feldspar, quartz, and melt to

balance the minor amount of water required by cordierite, giving rise to the full reaction shown in Fig. 10:



P-T conditions for this assemblage, therefore, lie on or below reaction [4] and between reactions [2] and [3], ca. 750 ± 30 °C and 3–4 kbar (Fig. 10b). This implies nearly isothermal decompression of about 2 kbar from peak conditions.

Thermobarometry of peak assemblage

Recovering more precise metamorphic *P-T* conditions using thermobarometry in granulite-facies rocks is a difficult task because of reequilibration by chemical diffusion upon cooling (e.g., Harley 1989; Pattison and Bégin 1994; Pattison et al.

Table 6. Metamorphic temperature estimations in footwall and hanging-wall rocks.

Thermometer (cation exchange)	Rock type	Sample #	Equilibrium	Calibration	<i>T</i> (°C)
Footwall					
Garnet–Biotite (Fe–Mg)	Paragneiss	GF-536	alm + phl = prp + ann	Bhattacharya et al. (1992)	756
	Paragneiss	GF-536	alm + phl = prp + ann	Dasgupta et al. (1991)	812
	Paragneiss	GF-536	alm + phl = prp + ann	Thompson (1976)	840
Garnet–Cordierite (Fe–Mg)	Paragneiss	GF-536	2 prp + 3 fcrd = 2 alm + 3 crd	Holland and Powell (1998)	825
Spinel–Cordierite (Fe–Mg)	Paragneiss	GF-536	2 spl + fcrd = 2 hc + crd	Nichols et al. (1992)	866
Hornblende–Plagioclase (Na–Ca)	Amphibolite	GF-273	ed + 4 qtz = tr + ab	Holland and Blundy (1994)	862
	Amphibolite	VC-17	ed + 4 qtz = tr + ab	Holland and Blundy (1994)	881
	Amphibolite	GF-273	ed + ab = ri + an	Holland and Blundy (1994)	805
	Amphibolite	VC-17	ed + ab = ri + an	Holland and Blundy (1994)	844
Hanging wall					
Garnet–Biotite (Fe–Mg)	Metasiltstone	VC-34	alm + phl = prp + ann	Bhattacharya et al. (1992)	441
	Metasiltstone	VC-34	alm + phl = prp + ann	Ferry and Spear (1978)	436
	Metasiltstone	VC-34	alm + phl = prp + ann	Thompson (1976)	470
Epidote (Fe)	Metasiltstone	VC-34	cz + fep = ep	Holland and Powell (1998)	415

Note: Mineral abbreviations from Holland and Powell (1998).

2003). Further complicating the situation is the completely altered state of the cordierite (with the exception of cordierite inclusions in late coronal spinel around garnet). Applying the “average *P–T*” method (Powell and Holland 1994) to the reduced assemblage of Grt–Bt–Pl–Sil–Qtz yields an estimate of 806 ± 195 °C and 7.0 ± 2.8 kbar (Table 7; Fig. 10*b*). To reduce the large uncertainty on the estimate, in particular for pressure, an estimated cordierite composition was added. Because stoichiometric Al and Si are virtually constant in cordierite, only the ratio of Fe/(Fe + Mg) has a significant effect on thermobarometry. Fe/(Fe + Mg) in cordierite was calculated to be in equilibrium with the measured garnet at 800 °C, the estimated temperature from phase equilibrium considerations. For sample GF-536, this resulted in a value of 0.30.

The average *P–T* in Table 7 is calculated based on the assemblage Grt–Crd–Bt–Sil–Qtz in sample GF-536. The grossular end member in garnet and the anorthite end member in plagioclase are not included for this *P–T* estimate because they significantly increase the uncertainty, suggesting that the measured compositions may not have been in equilibrium. The average *P–T* result, 804 ± 98 °C and 5.4 ± 0.9 kbar, produces a significantly more precise pressure estimate that is consistent with the phase equilibrium constraints of 800 ± 35 °C and 5.8 ± 0.6 kbar (Fig. 10*b*).

Temperature estimates using individual Fe–Mg exchange equilibria (Table 6) fall in the range 760–860 °C, averaging ca. 820 °C, similar to the abovementioned estimate. Temperatures obtained from hornblende–plagioclase thermobarometry in the metabasites (Table 6) lie in the range 800–880 °C, depending on the calibration applied.

Thermobarometry of late assemblage

The reaction-corona around mesosome garnet suggests a local chemical equilibrium among garnet, cordierite, spinel, sillimanite, quartz, and possibly melt. Compositions from the cordierite–spinel corona around garnet in sample GF-536 were used for *P–T* estimation. Cordierite is generally altered

but small unaltered inclusions are observed within spinel. For garnet, a mid-rim composition was selected, corresponding to the zone of lowest Mn content and highest Mg content. This domain lies inwards of the outer rim, where Mn content increases because of resorption and Mg content decreases because of late Fe–Mg exchange with neighbouring cordierite. The large garnet included within cordierite in the mesosome has a mid-rim composition that is the same as the rim composition of garnet within the leucosomes, which are included in quartz and do not have resorbed outer rims.

The calculated average *P–T* for this assemblage is 800 ± 90 °C at 4.2 ± 0.8 kbar (Table 7). Within the large uncertainties, this estimate is consistent with the 750 °C, 3–4 kbar constraint from phase equilibria (Fig. 10*b*).

Low-grade metamorphism in Quesnel terrane rocks

The metamorphosed sedimentary and volcanic rocks in the hanging wall of the Granby fault display a markedly lower grade of metamorphism than rocks in the footwall. Calcic metasiltstone locally contains manganiferous garnet, biotite, and epidote, while meta-andesite is characterized by the co-existence of actinolite and hornblende. These mineral assemblages are indicative of the transition between upper greenschist and lower amphibolite facies, corresponding to temperatures of 450–500 °C (Bégin 1992; Spear 1993) (Fig. 11). The variability of these bulk compositions and of the minerals contained in them (e.g., amphibole) makes more precise phase equilibrium constraints on the *P–T* conditions problematic. Thermobarometry was therefore attempted.

Thermobarometry in metasiltstone

Mineral compositions interpreted to be in equilibrium in the calcic metasiltstone VC-34 include rim compositions for garnet, epidote, and plagioclase and the average matrix biotite composition. To estimate peak temperature, calibrations of the garnet–biotite thermometer were applied to the sample.

Table 7. *P-T* results for footwall paragneiss and hanging-wall metasilstone using “AvePT” routine in THERMOCALC.

Sample	Mineral assemblage	End members (activities)	$a(\text{H}_2\text{O})$	<i>T</i> (°C)	<i>P</i> (kbar)	corr.	fit
Footwall							
GF-022	Peak : Grt-Bt-Pl-Sil-Qtz	At 800 °C: prp, grs, alm, phl, ann, east, an, sil, qtz	0.2	806±195	7.0±2.8	0.808	1.3
GF-536	Peak: Grt-Crd-Bt-Sil-Qtz (with generated Crd composition to fit expected temperature)	At 800 °C: prp, grs, alm, phl, ann, crd, fcrd, sil, qtz	0.2	804±98	5.4±0.9	0.848	0.41
GF-536	Late: Grt-Crd-Spl-Sil	At 800 °C: prp, grs, alm, ann, phl, spl, herc, crd, fcrd, sil, qtz	0.2	798±89	4.2±0.8	0.824	0.68
Hanging wall							
VC-34	Peak: Grt-Bt-Ep-Pl-Qtz-Rt-Ilm-H ₂ O	At 425 °C: pr, grs, alm, phl, ann, an, cz, ep, fep, rt, ilm	1	426±36	2.3 ±0.7	0.855	0.31

Note: Mineral abbreviations from Kretz (1983). Mineral endmember abbreviations from Holland and Powell (1998). Average *P-T* calculated with THERMOCALC 3.21, using the thermodynamic data of Holland and Powell (1998; 2002 update). For the footwall paragneiss, peak, and late assemblages are considered independently. The correlation (corr.) and fit numbers are statistical diagnostics defined by Powell and Holland (1994). Uncertainty is 1σ.

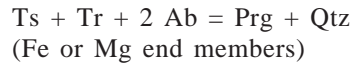
The results from various calibrations are similar, yielding an average temperature of ~450 ± 36 °C (Table 6; Fig. 11).

A set of four independent equilibria can be written for end members of the above phases in the chemical system CaKFMASH-Ti, therefore, allowing the use of the average *P-T* method of Powell and Holland (1994). Because of the absence of graphite, the mole fraction of water in the fluid phase is assumed to be 1. The statistical treatment yields a metamorphic *P-T* estimate of 426 ± 36 °C at 2.3 ± 0.7 kbar (Table 5; Fig. 11).

Thermobarometry in meta-andesite

In the meta-andesite, amphibole has a broad, continuous range of compositions from actinolite to hornblende, with both mineral species locally occurring in a close spatial and textural relationship (Fig. 9). The occurrence of hornblende, actinolite, and plagioclase of andesine composition, puts this assemblage at higher temperatures than the incoming of hornblende and oligoclase and at lower temperatures than the terminal stability of actinolite in mafic rocks (Fig. 11). The stability of hornblende-actinolite-oligoclase is restricted to temperatures between ~425 and 500 °C for pressures between 2 and 3 kbar, although these estimates carry considerable uncertainties.

More precise constraints were attempted by calculating the position of equilibria involving end members in amphibole and plagioclase in:

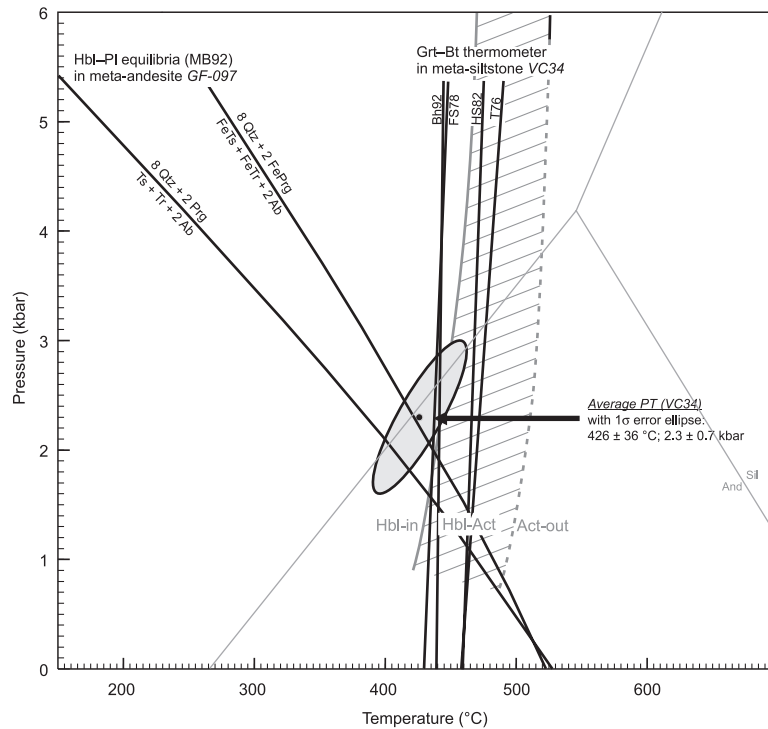


The average matrix amphibole composition and average rim composition of matrix plagioclase in sample GF-097 were used. The positions of the two reactions in *P-T* space, calculated with TWQ 1.02 (Berman 1991) using amphibole properties of Mader and Berman (1992), are plotted on Fig. 11. These results, combined with the epidote thermometer (Table 6), yield a *P-T* estimate of ~415 °C and 2.2 kbar, consistent with estimations from equilibria in the metasilstone.

U-Pb dating of monazite from the Grand Forks complex by LA-MC-ICP-MS

Monazite is a light rare-earth element (LREE) phosphate common in high-grade metapelitic rocks. Because its crystal structure incorporates a significant amount of Th and U, it is a good mineral for U-Pb dating, even when relatively young ages are expected. Monazite is also resistant to radiation damage from metamictization (Meldrum et al. 1998) and commonly displays negligible Pb diffusion and Pb loss (Parrish 1990). An initial “chemical dating” study of monazite from the GFC, using the electron microprobe, suggested a complex growth history reflected by compositional zoning and multiple age domains (Laberge 2005). Therefore, an in situ, high-resolution, precise, and accurate dating method was required to better define the age distribution. Laser ablation – multiple collector – inductively coupled plasma – mass spectrometry (LA-MC-ICP-MS) has been shown to produce precise and accurate apparent ages of accessory minerals (Horstwood et al. 2003; Simonetti et al. 2005). Because it is

Fig. 11. P - T diagram summarizing thermobarometry in hanging-wall rocks. The average P - T and 1σ error ellipse in metasiltstone was calculated in CKFMASH-Ti with the internally consistent thermodynamic data set of Holland and Powell (1998; 2002 update). Calibrations for the garnet-biotite thermometer are from Bhattacharya et al. (1992), Hodges and Spear (1982), Ferry and Spear (1978), and Thompson (1976). Selected equilibria in meta-andesite are based on calibrations of Mader and Berman (1992). The hornblende and actinolite boundaries are extrapolated from Bégin (1992).



gneiss, therefore, cannot be precisely estimated, but hypotheses can be made from textural observations and compositional variations. A correlation between age and chemical composition of the monazite has been documented in cases of multiple age populations, with Y content as a primary chemical variable (Foster et al. 2000; Pyle and Spear 2003; Spear 2004). A summary of interpretations of the monazite dates is presented in Table 9.

Generation 1

Generation 1 monazite (119 ± 4 Ma; $n = 1$) is the oldest observed generation and occurs as an inclusion near the core of a large garnet crystal in GF-536. This date is associated with a relatively high Y content (1.3 wt.%) and high Th/U ratio (~ 19), similar to monazites documented to have grown in other localities before or during the onset of garnet growth at lower amphibolite facies conditions (Pyle and Spear 2003; Yang and Pattison 2006). This age fits within a recognized period of major Early Cretaceous metamorphism and magmatism between 140 and 120 Ma (Parrish 1995; Digel et al. 1998; Crowley et al. 2000), during the early compressional stage of the orogeny, associated with the accretion of the allochthonous Intermontane terrane (Monger et al. 1982).

Generation 2

Generation 2 monazite (104 ± 3 Ma; $n = 3$) occurs within the core of two grains in GF-001. The three analysed locations have a similar chemical composition, with a high Y content (1.9 wt.%), and low Th/U ratio (~ 3.7). In the Valhalla

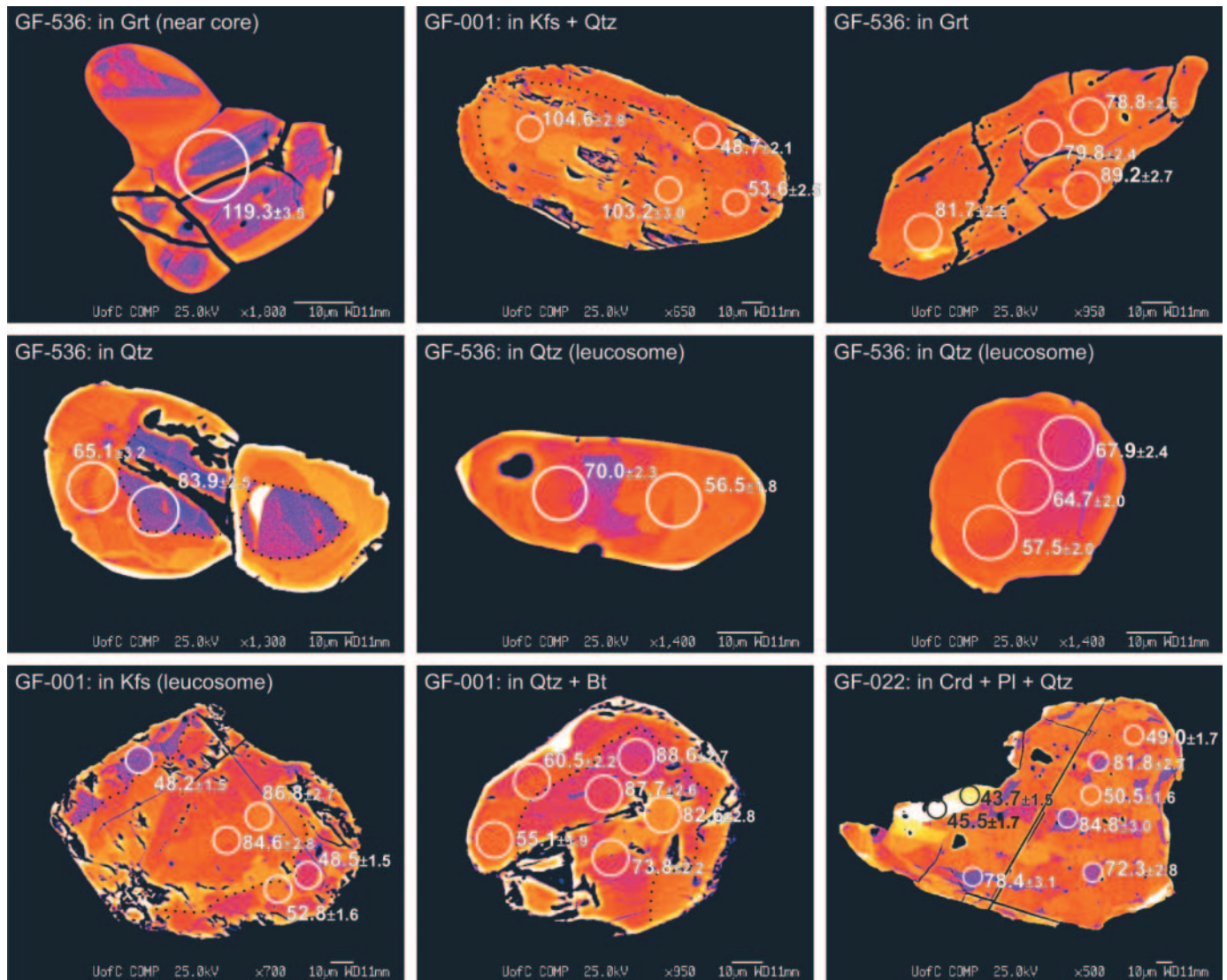
complex, 60 km to the northeast, Spear (2004) obtained a single monazite age of ~ 105 Ma, which he ascribed to an episode of contact metamorphism, as it is synchronous with the crystallization age of the protoliths of two orthogneisses (Spear and Parrish 1996). This thermal episode is roughly synchronous with ~ 110 Ma monazite inclusions in garnet in the Mica Creek area, located between the Monashee complex and the Malton gneiss (Crowley et al. 2000) and with ~ 100 Ma upper amphibolite metamorphism and pegmatite crystallization in the northern Monashee Mountains (Sevigny et al. 1990; Scammell and Dixon 1993; Parrish 1995) and the Frenchman Cap of the Monashee complex (Gilley et al. 2000).

Generation 3

Generation 3 monazite (mean: 84 ± 3 Ma; range: 89 ± 3 to 78 ± 3 Ma; $n = 17$) is the dominant population of monazite in the GFC. It occurs within the core of matrix grains and within an inclusion in garnet. Monazite in this group has a rather broad compositional range (Fig. 14). The distribution of this dominant age population (Fig. 13) suggests prograde Cretaceous metamorphism starting at about 89 Ma and extending to about 78 Ma, similar to the 85–75 Ma episode of prograde metamorphism in the Valhalla complex (Spear 2004) and monazite growth in the core of matrix grains in parts of the Mica Creek area (Crowley et al. 2000).

Between Generation 3 and younger generations, there is a sharp compositional contrast implied by the contrast in BSE intensity (Fig. 12). The allomorphic shape of generation 3 monazite crystals, with rounded and globular edges, suggests

Fig. 12. Back-scattered electron images of selected monazite crystals from the Grand Forks paragneiss showing the location of the 12 μm ablation pits and their corresponding apparent $^{207}\text{Pb}/^{206}\text{Pb}$ age and 2σ error (Ma). See Table 8 for details. Grayscale has been converted to a colour scheme to increase contrast (see web version of the paper for colour). Dashed lines outline limits of compositional zones.



dissolution or resorption before the growth of younger generations of monazite.

Generation 4

Generation 4 monazite (range 74–56 Ma; $n = 12$) occurs as rims and patches around generation 3 monazite and in two small inclusions (one euhedral) in quartz within leucosomes. It is not clear whether these dates represent an actual growth period or represent mixed ages because of the overlap of the laser beam across growth domains, or both. Many of these analyses are texturally located in rims and small patches smaller than the size of the laser beam (e.g., Fig. 12, grains #3, #13). It is, thus, quite likely that some of these dates represent a mixture between age domains. However, five of these analyses, ranging from 70.0 ± 2.3 to 56.5 ± 1.8 Ma, associated with low Y content, were obtained from two discrete grains enclosed in quartz within leucosomes in GF-536. As monazite can grow during crystal-

lization of partial melt (e.g., Pyle and Spear 2003), it is possible that these ages, as young as 56.5 ± 1.8 Ma, represent the age of leucosome crystallization. However, a hornblende K–Ar age indicates cooling to 530 ± 30 °C at 60 ± 1 Ma (Hunt and Roddick 1990), well below the solidus temperature for these rocks. Thus, these ages remain enigmatic. Interestingly, Parrish (1992) obtained a 56 ± 1 Ma U–Pb igneous crystallization age for biotite leucogranite intruded within the GFC ~40 km north of the study area (Fig. 1). These ages are also consistent with the regionally extensive 59–55 Ma Ladybird leucogranite in the Monashee complex (Carr 1992).

Generation 5

Generation 5 monazite (51 ± 2 Ma; $n = 11$) is characterized by a broad range of Y-content but well constrained Th/U ratio within samples. It occurs as rims around, or as recrystallized patches in, monazite grains located along the grain bound-

Table 8. U–Pb laser ablation dating results for monazite from the GFC.

Sample	Analysis #	Electron microprobe data (ppm)					LA–MC–ICP–MS isotopic ratio				Apparent ages (Ma)			
		Th	U	Pb	Y	Th/U	$\frac{^{207}\text{Pb}}{^{235}\text{U}}$	$\pm 2\sigma$	$\frac{^{206}\text{Pb}}{^{238}\text{U}}$	$\pm 2\sigma$	$\frac{^{206}\text{Pb}}{^{238}\text{U}}$	$\pm 2\sigma$	$\frac{^{207}\text{Pb}}{^{206}\text{Pb}}$	$\pm 2\sigma$
536	10	68169	3605	446	13095	18.9	0.1250	0.0041	0.01859	0.00066	118.7	4.2	119.3	3.5
001	15	29967	8145	288	19347	3.7	0.1077	0.0036	0.01606	0.00079	102.7	5.0	104.6	2.8
001	21	26795	7052	232	19363	3.8	0.1080	0.0037	0.01619	0.00061	103.6	3.9	104.0	3.2
001	12	28043	7325	288	18820	3.8	0.1064	0.0035	0.01589	0.00075	101.6	4.8	103.2	3.0
536	7	35152	4637	241	14843	7.6	0.0918	0.0030	0.01394	0.00043	89.2	2.8	89.2	2.7
001	27	30969	7528	269	21064	4.1	0.0909	0.0030	0.01355	0.00053	86.8	3.4	89.0	2.7
001	35	37376	2935	167	19899	5.6	0.0914	0.0031	0.01378	0.00046	88.3	2.9	88.6	2.7
001	23	33878	5157	204	5536	4.3	0.0905	0.0036	0.01374	0.00065	88.0	4.1	88.0	3.1
001	40	34757	6215	288	19458	9.3	0.0898	0.0029	0.01356	0.00054	86.8	3.4	87.7	2.6
001	3	43914	10128	399	25127	6.1	0.0894	0.0029	0.01349	0.00046	86.4	2.9	86.8	2.7
022	24	42227	4522	279	24552	5.2	0.0871	0.0033	0.01312	0.00067	84.0	4.3	84.8	3.0
001	2	35592	5827	260	22222	7.0	0.0867	0.0034	0.01323	0.00052	84.7	3.3	84.6	2.8
001	24	33166	5130	176	4921	9.0	0.0870	0.0043	0.01297	0.00103	83.1	6.6	84.6	4.0
536	23	46067	8894	316	18064	9.6	0.0864	0.0029	0.01319	0.00055	84.5	3.5	83.9	2.5
001	34	40689	6638	214	6937	10.3	0.0848	0.0031	0.01285	0.00052	82.3	3.3	82.6	2.8
022	25	39986	5694	279	23119	4.6	0.0839	0.0029	0.01273	0.00053	81.6	3.4	81.8	2.7
536	5	54143	5985	288	22316	6.7	0.0845	0.0028	0.01266	0.00041	81.1	2.6	81.7	2.5
001	28	38483	6902	251	3323	6.4	0.0832	0.0030	0.01233	0.00058	79.0	3.7	81.2	2.8
536	8	54732	5686	241	23450	12.7	0.0833	0.0030	0.01233	0.00040	79.0	2.6	79.8	2.4
536	9	63555	6170	325	25529	6.6	0.0807	0.0032	0.01230	0.00047	78.8	3.0	78.8	2.6
022	28	29800	6435	214	24001	6.5	0.0806	0.0033	0.01200	0.00065	76.9	4.2	78.4	3.1
022	9	46542	1798	139	30505	6.1	0.0759	0.0028	0.01158	0.00037	74.2	2.4	74.2	2.3
001	33	35284	6911	158	19489	5.6	0.0745	0.0028	0.01118	0.00066	71.7	3.5	73.8	2.2
022	23	39397	5906	288	24348	25.9	0.0739	0.0030	0.01123	0.00055	72.0	3.6	72.3	2.8
001	31	44169	11830	288	7819	5.1	0.0716	0.0025	0.01092	0.00065	70.0	4.2	70.2	2.3
536	16	66297	3597	269	2858	3.7	0.0716	0.0025	0.01087	0.00038	69.7	2.4	70.0	2.3
536	3	29554	9115	195	9497	18.4	0.0711	0.0047	0.01053	0.00039	67.5	2.5	67.9	2.4
536	25	67246	4504	241	5008	3.2	0.0663	0.0071	0.01015	0.00051	65.1	3.5	65.1	3.2
536	1	43940	7070	223	6528	14.9	0.0653	0.0025	0.01011	0.00033	64.9	2.1	64.7	2.0
022	14	46533	1895	167	34450	6.2	0.0626	0.0027	0.00966	0.00031	62.0	2.0	61.9	1.9
001	39	37929	6761	195	13875	24.6	0.0614	0.0023	0.00934	0.00096	59.9	6.1	60.5	2.2
536	2	49767	6664	251	6733	5.6	0.0587	0.0022	0.00890	0.00032	57.1	2.1	57.5	2.0
536	15	64338	2354	176	1575	7.5	0.0554	0.0029	0.00886	0.00029	56.9	1.9	56.5	1.8
001	38	38202	7008	139	12465	27.3	0.0546	0.0023	0.00818	0.00050	52.5	3.2	55.1	1.9
001	30	37437	6955	176	11867	5.5	0.0553	0.0021	0.00851	0.00033	54.6	2.1	54.6	2.0
001	10	31540	5263	167	21851	5.4	0.0544	0.0031	0.00834	0.00043	53.5	2.8	53.6	2.5
001	7	37121	6074	204	10536	6.0	0.0531	0.0026	0.00822	0.00026	52.8	1.7	52.8	1.6
001	19	34599	5404	204	19969	6.1	0.0527	0.0023	0.00785	0.00031	50.4	2.0	50.9	1.9
022	18	44775	2680	93	5599	16.7	0.0495	0.0022	0.00786	0.00025	50.5	1.6	50.5	1.6
001	26	38553	4187	121	20229	9.2	0.0500	0.0031	0.00756	0.00069	48.6	4.4	49.8	2.8
022	15	43888	3165	158	7205	13.9	0.0479	0.0027	0.00764	0.00026	49.1	3.5	49.0	1.7
001	13	31848	5095	139	21812	6.3	0.0492	0.0021	0.00781	0.00064	50.2	4.1	48.7	2.1
001	6	37552	3905	111	25867	9.6	0.0487	0.0021	0.00755	0.00024	48.5	1.5	48.5	1.5
022	30	34634	4002	158	28521	8.7	0.0496	0.0031	0.00751	0.00024	48.2	1.5	48.2	1.5
001	9	154969	2257	325	19710	68.7	0.0468	0.0022	0.00707	0.00027	45.4	1.7	45.5	1.7
022	29	86413	1860	195	22442	46.5	0.0446	0.0052	0.00680	0.00024	43.7	1.6	43.7	1.5

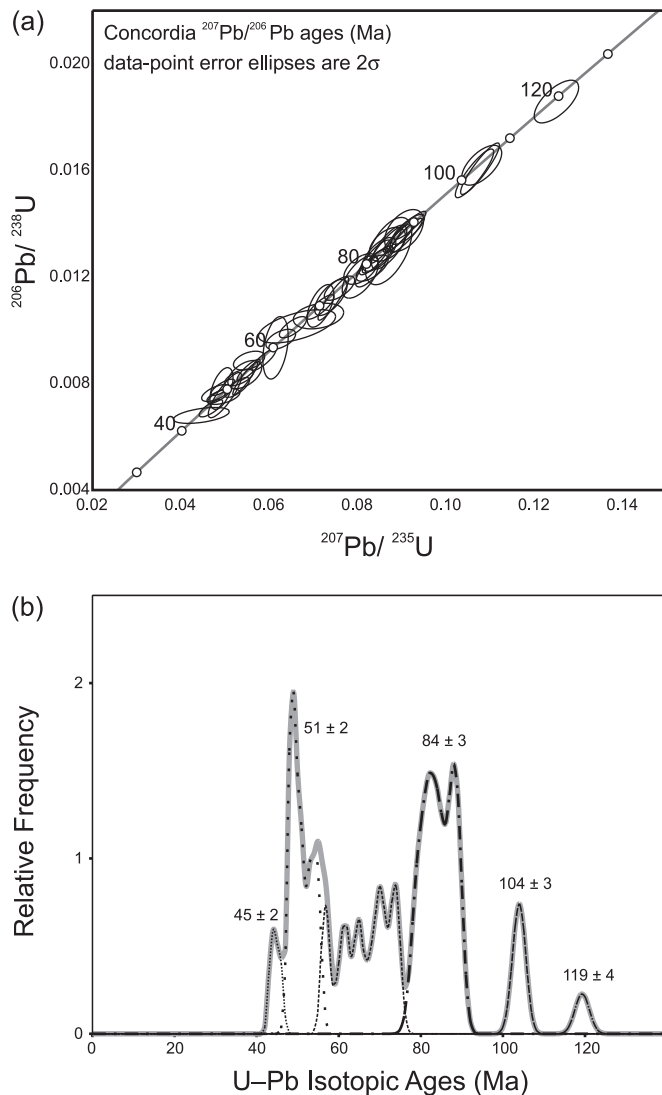
Note: Lines separate age groups discussed in text.

Table 9. Summary and interpretations of the multiple monazite age generations from the GFC.

Generation	<i>n</i>	Weighted mean of $^{207}\text{Pb}/^{206}\text{Pb}$ monazite dates					Interpretation
		Mean	2σ	Maximum	Minimum	MSWD	
1	1	119.3	3.5	119.3 ± 3.5	119.3 ± 3.5	0.00	Early metamorphic event at 119.3 ± 3.5 Ma
2	3	104.0	3.0	104.6 ± 2.8	103.2 ± 3.0	0.16	Early contact metamorphic(?) event at 104.0 ± 3.0 Ma
3	17	84.1	2.8	89.2 ± 2.7	78.4 ± 3.1	6.59	Prograde metamorphism from ~89 to 78 Ma
4	12	65.2	2.3	74.2 ± 2.3	56.5 ± 1.8	31.07	Some mixed ages, leucosome crystallization(?) at 56.5 ± 1.8 Ma
5	11	50.8	2.0	55.1 ± 1.9	48.2 ± 1.5	6.98	Recrystallization during a Coryell-related thermal event at 50.8 ± 2.0 Ma
6	2	44.5	1.6	45.5 ± 1.7	43.7 ± 1.5	1.26	Hydrothermal recrystallization (?) at 44.5 ± 1.6 Ma

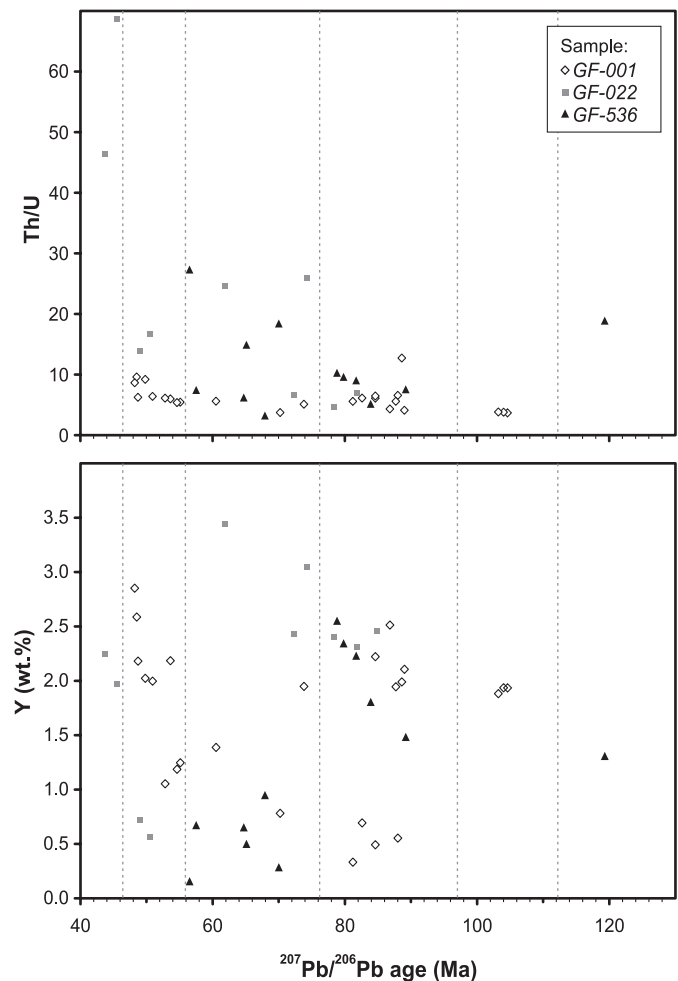
Note: Dates in Ma. MSWD, mean square of weighted deviates.

Fig. 13. Monazite U–Pb isotopic ages from 46 analyses on 12 grains from the Grand Forks paragneiss, acquired by LA–MC–ICP–MS. (a) Concordia diagram showing the 2σ error ellipses; (b) Relative distribution of ages plotted as the sum of their normal distributions (thick line), and separated into six age groups (dashed lines).



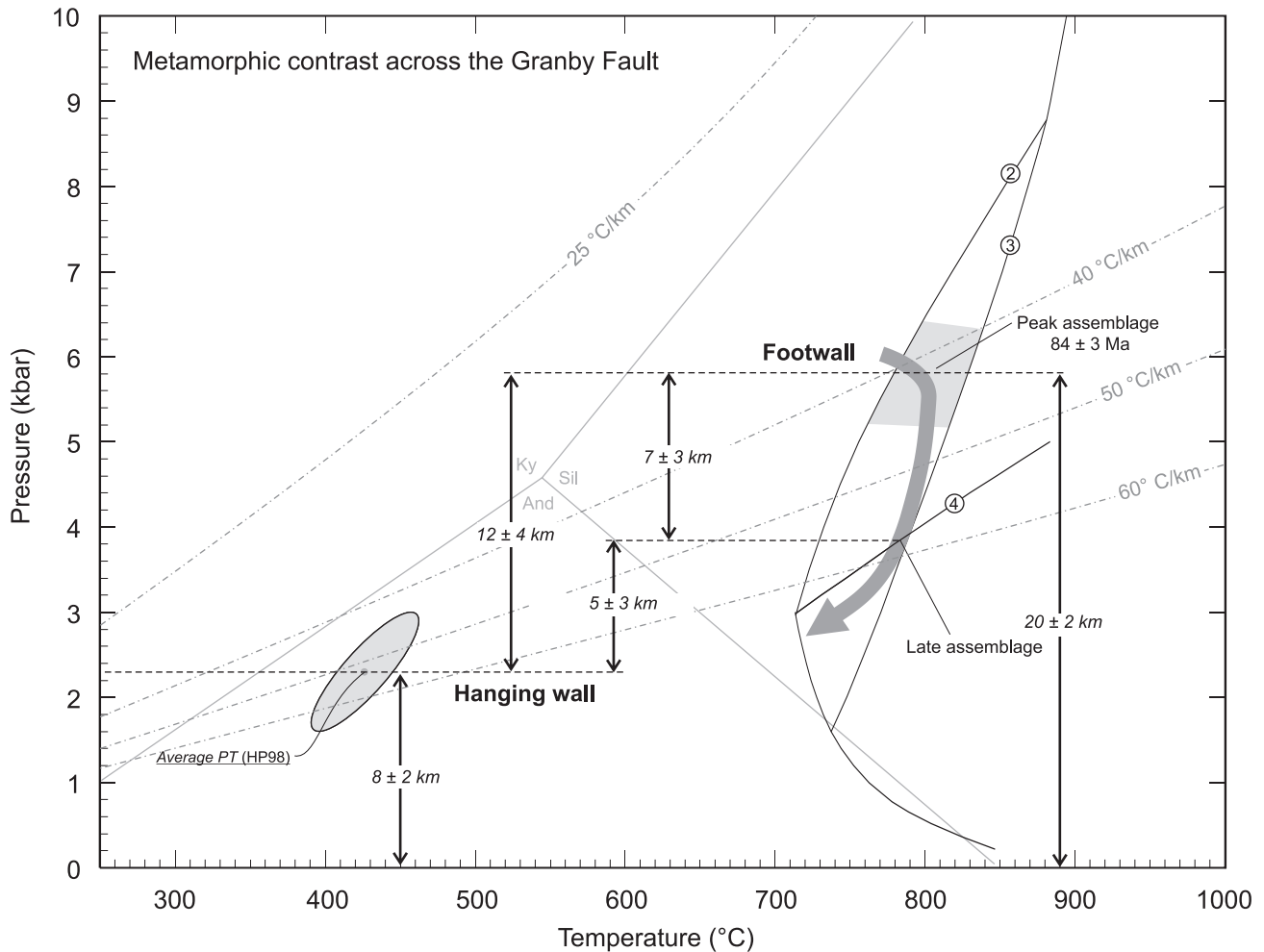
aries of matrix minerals (i.e., monazite grains not occurring as inclusions). This observation suggests the possibility of interaction with an intergranular hydrothermal fluid. An

Fig. 14. Variation in Y content and Th/U ratio in monazite from three paragneiss samples from the Grand Forks complex. Dashed lines separate age groups discussed in text.



Eocene thermal event, causing high heat flow and high-level plutonism, is well recorded in the southern Omineca belt (Parrish 1995). The Coryell intrusive suite, which borders the complex in the map area, yields a crystallization age of 51.1 ± 0.5 Ma (Carr and Parkinson 1989). Thus, it seems likely that generation 5 monazite is related to either or both of thermal or hydrothermal processes concomitant with the intrusion of the nearby Coryell batholith.

Fig. 15. *P-T* diagram summarizing metamorphic conditions in the hanging-wall and footwall rocks of the Granby Fault. Steady-state geothermal gradients are calculated using the method of Spear (1993) assuming uniform heat production of $0.75 \mu\text{Wm}^{-3}$, a mantle heat flux of 30 mWm^{-2} , a thermal conductivity of $2.25 \text{ Wm}^{-1}\text{K}^{-1}$ and a uniform crustal density of 2.85 gcm^{-3} , based on average crustal values of Spear (1993). Labels for geothermal gradients are values at a depth of 10 km. Depth conversion 1 kbar = 3.4 km.



Generation 6

Generation 6 monazite ($45 \pm 2 \text{ Ma}$; $n = 2$) occurs locally as a thin outer rim, thick enough for analysis only in a single grain. The Th/U ratio (46–59) is much higher than any other monazite. Interaction with a hydrothermal fluid associated with a felsic intrusion could account for the high Th content of this late monazite, but the significance of this age remains unknown.

Protracted Cretaceous metamorphism in the Grand Forks complex

U–Pb data acquired by LA–MC–ICP–MS suggests monazite growth during Early Cretaceous metamorphic events at 119 ± 4 and $104 \pm 3 \text{ Ma}$, followed by a dominant Late Cretaceous regional prograde metamorphic event at $84 \pm 3 \text{ Ma}$. A cryptic event occurs at $57 \pm 2 \text{ Ma}$, followed by two Eocene events (51 ± 2 and $44 \pm 1 \text{ Ma}$), the first of which is likely related to intrusion of the Coryell batholith.

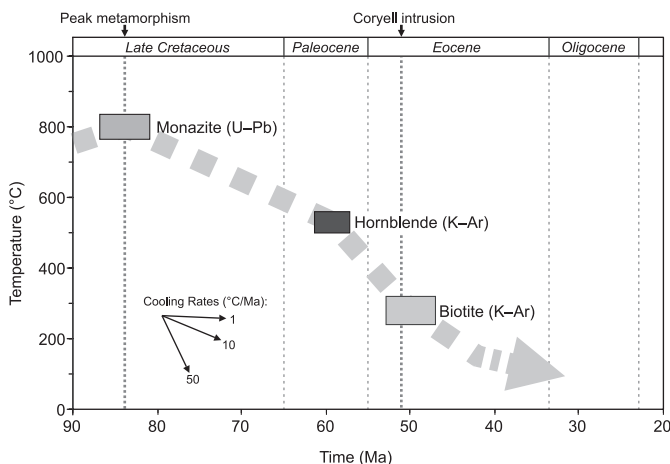
The GFC can, therefore, be included in a widespread zone of Late Cretaceous to early Tertiary regional metamorphism and penetrative deformation in the southern Canadian Cordillera. Metamorphism of this age has been recognized

throughout the southern Omineca belt, including the northern Monashee Mountains just south of the Malton gneiss (Sevigny et al. 1990), the Monashee complex (Scammell and Dixon 1993; Gibson et al. 1999; Gilley et al. 2000; Teyssier et al. 2005), parts of the Selkirk allochthon (Johnston et al. 2000) and the Valhalla complex (Schaubs and Carr 1998; Spear 2004). The Late Cretaceous orogenic belt extends as far west as the Vernon antiform (Glombick et al. 2005) and the GFC.

Pressure–temperature contrast across the Granby fault

Peak Late Cretaceous metamorphic conditions in the GFC are estimated from phase equilibria to be $800 \pm 35 \text{ }^\circ\text{C}$ and $5.8 \pm 0.6 \text{ kbar}$, consistent with the average *P-T* thermobarometry estimate of $804 \pm 98 \text{ }^\circ\text{C}$ and $5.4 \pm 0.9 \text{ kbar}$. Phase equilibrium constraints on late cordierite-spinel coronal assemblages indicate conditions of $750 \pm 30 \text{ }^\circ\text{C}$ and 3–4 kbar, consistent within error with the average *P-T* estimate of $800 \pm 90 \text{ }^\circ\text{C}$ and $4.2 \pm 0.8 \text{ kbar}$. Examining Fig. 15, the difference between the two indicates approximately isothermal

Fig. 16. Cooling history of the Grand Forks complex based on published K–Ar thermal ages and U–Pb monazite dating from this study. See text for details. K–Ar closure temperatures are 530 ± 30 °C for hornblende (Harrison 1981) and 280 ± 40 °C for biotite (Harrison et al. 1985).



decompression from peak conditions of ca. 2 kbar. Placing a meaningful uncertainty on this estimate is difficult, but it is likely to be $\leq \pm 1$ kbar.

Assuming a uniform crustal density of $2.85 \text{ g}\cdot\text{cm}^{-3}$ (3.4 km/kbar), rocks of the complex now exposed at the surface were at a mid-crustal depth of $20 \pm 2 \text{ km}$, by $84 \pm 3 \text{ Ma}$. They were then exhumed by $7 \pm 3.5 \text{ km}$ while remaining at temperatures > 750 °C, before cooling and further exhumation. High-temperature decompression has been reported within other metamorphic core complexes in the southern Omineca belt. For example, Norlander et al. (2002) have interpreted 3–6 kbar of isothermal decompression (from 8–10 kbar to 4–5 kbar) at 750 °C in the southern part of the Monashee complex. No evidence for significant decompression has been observed in the Valhalla complex (Schaubs et al. 2002; Spear 2004).

Rocks in the hanging wall of the Granby fault reached metamorphic pressures of $2.3 \pm 0.7 \text{ kbar}$, indicating $8 \pm 2.5 \text{ km}$ of post-metamorphic denudation. Because of the uncertainties regarding the timing of metamorphism in these rocks, it is not clear whether this amount of denudation has taken place since the Late Cretaceous or since the accretion of these rocks to North America in the Middle Jurassic.

The P – T contrast between peak metamorphic conditions in the hanging wall and footwall of the Granby fault is, therefore, on the order of 375 ± 70 °C and $3.5 \pm 1.3 \text{ kbar}$ (Fig. 15), corresponding to a vertical depth contrast of $12 \pm 4.5 \text{ km}$. The metamorphic pressure contrast between the hanging-wall and footwall rocks after high-temperature decompression is $1.5 \pm 1.0 \text{ kbar}$, or $5 \pm 3.5 \text{ km}$ (Fig. 15). This high-temperature decompression is associated with a marked rise of the isothermal gradient, from ~ 40 – 45 °C/km during peak conditions to ~ 55 – 60 °C/km after decompression (Fig. 15). Determining the role of the Granby fault in the exhumation of the complex requires information on the cooling history of the GFC.

Cooling history of the GFC with implications for displacement on the Granby fault

The cooling history of the complex can be inferred from published data combined with U–Pb monazite ages from this study. Published chronological data in the vicinity of the GFC are reported in Table 1 and Fig. 1b, and a T – t (temperature–time) diagram is presented in Fig. 16. Two hornblende K–Ar ages are documented within the GFC (Table 1; Fig. 1) (Stevens et al. 1982; Hunt and Roddick 1990). The two reported ages from the same locality, 2.5 km north of Grand Forks, yield a weighted mean of $60.5 \pm 2.1 \text{ Ma}$. Three biotite K–Ar ages from the GFC have been previously published (Table 1; Fig. 1) (Wanless et al. 1979; Addie 1980; Stevens et al. 1983), yielding a weighted mean of $49.9 \pm 2.9 \text{ Ma}$. The resulting cooling curve suggests an average cooling rate of ~ 11 °C/Ma from 84 to 60 Ma, increasing to ~ 25 °C/Ma from 60 to 50 Ma. The increasing cooling rate during the Tertiary is attributed to increased denudation rates during crustal extension and normal faulting.

Crosscutting relationships between the Granby fault and the Coryell intrusions indicate at least some post-51 Ma displacement on the fault, at a time when the GFC would have already cooled to 400–300 °C (Fig. 16). Combined with the brittle nature of the fault, this suggests that the fault is a late structure that developed after the core complex had already cooled significantly. The onset of regional extension is believed to be $\sim 58 \text{ Ma}$ in the southern Canadian Cordillera (Carr et al. 1987), at which time the complex would have already cooled to temperatures lower than ~ 550 °C (Fig. 16).

The throw on the Granby fault is, therefore, estimated to be $5 \pm 3.5 \text{ km}$. This estimate is a minimum because it assumes synchronous metamorphism of hanging-wall and footwall rocks. If hanging-wall metamorphism was pre-Cretaceous, the throw could be as much as $9 \pm 2 \text{ km}$ (from conditions of 3–4 kbar after decompression, assuming a minimum of 3 km of post-84 Ma erosion, as indicated by the presence of coarse Eocene intrusive rocks in the area). A minimum 5 km estimate is in excellent agreement with the minimum 4–6 km estimate from stratigraphic considerations (Fyles in Roback et al. 1995), suggesting that the lower end of the range permitted by the uncertainties, 1.5 km, is too small.

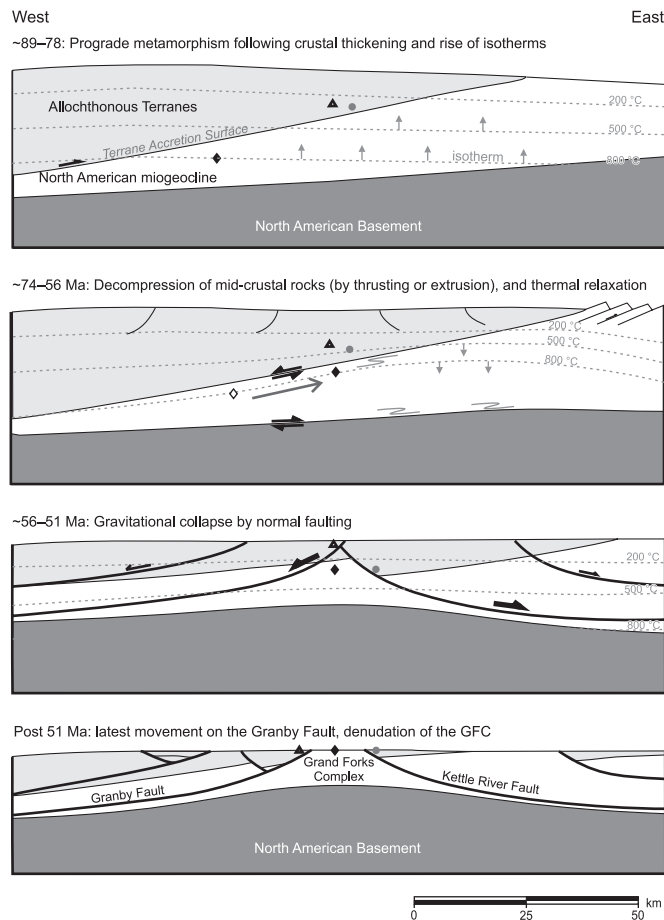
Nevertheless, 5 km of vertical displacement on the Granby fault is rather less than might be surmised from the striking metamorphic contrast across the fault. Assuming the fault dips about 30°, the horizontal displacement component would be 8–9 km along a flat fault plane and around 6–7 km on a listric surface flattening in the lower crust.

Causes of high-temperature decompression in the GFC

The amount of displacement on the Granby fault does not account for the early high-temperature decompression of $2 \pm 1 \text{ kbar}$ of the core complex in the Late Cretaceous. Considering that this event occurred in a broad compression regime in the Omineca belt, possibilities include thrust-duplexing, channel flow in the middle crust, or normal faulting in the upper crust during mid-crustal compression.

In the Valhalla complex, thrusting along a deep-seated ramp is the mechanism favoured by Spear and Parrish

Fig. 17. Schematic cross-sections at the latitude of Volcanic Creek at four different time intervals, illustrating the exhumation of the Grand Forks complex (GFC), driven by Late Cretaceous orogenesis, followed by Paleocene to Eocene crustal extension. The evolution of three rocks (one in the footwall, two in the hanging wall to the Granby and Kettle River faults) is represented by the three different symbols. Plutonic rocks are ignored for simplicity. The east-dipping Kettle River fault is slightly older than the Granby fault, as the Coryell suite intrudes the Kettle River fault, but is cut by the Granby fault (Fig. 1).



(1996), Schaub et al. (2002), and Spear (2004) to account for very rapid cooling immediately following peak metamorphism. According to thermal models, such a thrusting mechanism could result in very high cooling rates, >100 °C/Ma, even for rocks several kilometres away from the thrust plane and nearly isobaric cooling following peak metamorphism (Spear 2004). Such a *P–T* path is opposite to that documented for the GFC, which involves high-temperature decompression followed by moderately rapid cooling. However, a thrusting mechanism cannot be ruled out since increasing the distance of the GFC from a cooler lower plate by a few kilometres would significantly delay cooling and might provide consistency with our observations.

Ductile flow of mid-crustal rocks by either diapirism (vertical flow) (Teyssier and Whitney 2002; Whitney et al. 2004), channel flow (lateral flow), or a combination of the two (Brown and Gibson 2005), is another compressional mechanism suggested for tectonic uplift of core complexes.

In the Monashee complex, lateral and upward flow or extrusion of hot and ductile mid-crustal rocks was argued by Johnston et al. (2000), while Norlander et al. (2002) proposed a diapiric model to account for the isothermal decompression in the Thor-Odin dome.

The interpreted near-isothermal decompression of the GFC, followed by moderately rapid cooling, suggests decoupling between the mid-crustal block and the upper plate during that initial decompression. A conceptual model is presented in Fig. 17. The Late Cretaceous exhumation of mid-crustal rocks could have occurred within a metasedimentary wedge between the allochthonous terranes and the North American basement. In this scenario, the most likely decoupling surface would be the terrane accretion boundary. Alternatively, normal faulting in the upper crust, in a deeper compressional setting, might account for some of the initial mid-crustal decompression. Improved structural evidence will be needed to better constrain the cause of the Late Cretaceous to Paleocene exhumation of the Grand Forks complex prior to normal faulting on the Granby fault.

Acknowledgements

Research funding was provided by Natural Sciences and Engineering Research Council grant No. 0037233 to D.R.M.P. Thanks to Phil Simony for his involvement in this project and for insightful discussions. Scott McLaren provided efficient field assistance during the summer of 2003. Doug Tinkham is thanked for scientific and technical support with thermobarometric issues. We are grateful to Tom Chacko and Tony Simonetti for their help in the acquisition of LA-MC-ICP-MS data. Sharon Carr and Frank Spear provided helpful reviews of the paper.

References

Addie, G.G. 1980. Mineral Property Examinations: Southeast British Columbia, DEB (SD 18). *In* Geological Fieldwork 1979. British Columbia Geological Division, Paper 1980-1, pp. 112–113.

Armstrong, R.L., Parrish, R.R., van der Heyden, P., Scott, K., Runkle, D., and Brown, R.L. 1991. Early Proterozoic basement exposures in the southern Canadian Cordillera; core gneiss of Frenchman Cap, Unit I of the Grand Forks Gneiss, and the Vaseaux Formation. *Canadian Journal of Earth Sciences*, **28**: 1169–1201.

Baadsgaard, H., Folinsbee, R.E., and Lipson, J.I. 1961. Potassium–argon dates of biotites from Cordilleran granites. *Geological Society of America Bulletin*, **72**(5): 689–701.

Bégin, N.J. 1992. Contrasting mineral isograd sequences in metabasites of the Cape Smith belt, northern Québec, Canada: three new bathograds for mafic rocks. *Journal of Metamorphic Geology*, **10**: 685–704.

Berman, R.G. 1991. Thermobarometry using multiequilibrium calculations: a new technique with petrologic applications. *Canadian Mineralogist*, **29**: 833–855.

Bhattacharya, A., Mohanty, L., Maji, A., Sen, S.K., and Raith, M. 1992. Non-ideal mixing in the phlogopite–annite binary; constraints from experimental data on Mg–Fe partitioning and a reformulation of the biotite–garnet geothermometer. *Contributions to Mineralogy and Petrology*, **111**(1): 87–93.

Breitsprecher, K., and Mortensen, J.K. 2004. BCAGE 2004A — a database of isotopic age determinations for rock units from British

- Columbia. British Columbia Ministry of Energy and Mines, Open File 2004-3 (Release 3.0), 7757 records, 9.3 Mb.
- Brown, R.L., and Journeay, J.M. 1987. Tectonic denudation of the Shuswap metamorphic terrane of southeastern British Columbia. *Geology*, **15**(2): 142–146.
- Carr, S.D. 1992. Tectonic setting and U–Pb geochronology of the early Tertiary Ladybird leucogranite suite, Thor–Odin–Pinnacles area, southern Omineca belt, British Columbia. *Tectonics*, **11**(2): 258–278.
- Carr, S.D., and Parkinson, D.L. 1989. Eocene stratigraphy, age of the Coryell Batholith, and extensional faults in the Granby Valley, southern British Columbia. Geological Survey of Canada, Paper 89-1E, pp. 79–87.
- Carr, S.D., Parrish, R.R., and Brown, R.L. 1987. Eocene structural development of the Valhalla Complex, southeastern British Columbia. *Tectonics*, **6**(2): 175–196.
- Cheney, E.S. 1980. Kettle dome and related structures of northeastern Washington. In *Cordilleran metamorphic core complexes*. Edited by M.D. Crittenden, P.S. Coney and G.H. Davis. Geological Society of America, Memoir 153, pp. 463–483.
- Church, B.N. 1986. Geological setting and mineralization in the Mount Attwood – Phoenix area of the Greenwood mining camp. British Columbia Ministry of Energy, Mines and Petroleum Resources, Paper 1986-2.
- Crowley, J.L., Ghent, E.D., Carr, S.D., Simony, P.S., and Hamilton, M.A. 2000. Multiple thermotectonic events in a continuous metamorphic sequence, Mica Creek area, southeastern Canadian Cordillera. *Geological Materials Research*, **2**(2): 1–46.
- Dasgupta, S., Sengupta, P., Guha, D., and Fukuoka, M. 1991. A refined garnet–biotite Fe–Mg exchange geothermometer and its application in amphibolites and granulites. *Contributions to Mineralogy and Petrology*, **109**(1): 130–137.
- Digel, S.G., Ghent, E.D., Carr, S.D., and Simony, P.S. 1998. Early Cretaceous kyanite–sillimanite metamorphism and Paleocene sillimanite overprint near Mount Cheadle, southeastern British Columbia; geometry, geochronology, and metamorphic implications. *Canadian Journal of Earth Sciences*, **35**(9): 1070–1087.
- Ferry, J.M., and Spear, F.S. 1978. Experimental calibration of the partitioning of Fe and Mg between biotite and garnet. *Contributions to Mineralogy and Petrology*, **66**(2): 113–117.
- Foster, G., Kinny, P., Vance, D., Prince, C., and Harris, N. 2000. The significance of monazite U–Th–Pb age data in metamorphic assemblages; a combined study of monazite and garnet chronometry. *Earth and Planetary Science Letters*, **181**(3): 327–340.
- Fyles, J.T. 1990. Geology of the Greenwood – Grand Forks area, British Columbia; NTS 82E/ 1.2. British Columbia Ministry of Energy, Mines and Petroleum Resources, Open File 1990-25.
- Gabrielse, H., Monger, J.W.H., Wheeler, J.O., and Yorath, C.J. 1991. Morphogeological belts, tectonic assemblages, and terranes. In *Geology of the Cordilleran Orogen in Canada*. Edited by H. Gabrielse and C.J. Yorath. Geological Survey of Canada, Geology of Canada, no. 4, Chap. 2, Part A, pp. 13–59.
- Gibson, H.D., Brown, R.L., Parrish, R.R., 1999. Deformation-induced inverted metamorphic field gradients: an example from the southeastern Canadian Cordillera. *Journal of Structural Geology*, **21**(7): 751–767.
- Gilley, L., Ireland, T., Norlander, B., and Stockli, D. 2000. SHRIMP U–Pb dating of partial melting in the Shuswap Complex, British Columbia. Geological Society of America, Abstracts with Programs, **32**(7), pp. 170.
- Glombick, P., Thompson, R.I., Erdmer, P., Heaman, L., Friedman, R.M., Villeneuve, R., and Daughtry, K.L. 2005. U–Pb constraints on the thermotectonic evolution of the Vernon antiform and the age of the Aberdeen gneiss complex, southeastern Canadian Cordillera. *Canadian Journal of Earth Sciences*, **43**: 213–244.
- Harley, S.L. 1989. The origins of granulites: a metamorphic perspective. *Geological Magazine*, **126**: 215–247.
- Harley, S.L., Thompson, P., Hensen, B.J., and Buick, I.S. 2002. Cordierite as a sensor of fluid conditions in high-grade metamorphism and crustal anatexis. *Journal of Metamorphic Geology*, **20**(1): 71–86.
- Harrison, T.M. 1981. Diffusion of ⁴⁰Ar in hornblende. *Contributions to Mineralogy and Petrology*, **78**(3): 324–331.
- Harrison, T.M., Duncan, I., and McDougall, I. 1985. Diffusion of (super 40) Ar in biotite; temperature, pressure and compositional effects. *Geochimica et Cosmochimica Acta*, **49**(11): 2461–2468.
- Hodges, K.V., and Spear, F.S. 1982. Geothermometry, geobarometry and the Al₂SiO₅ triple point at Mt. Moosilauke, New Hampshire. *American Mineralogist*, **67** (11–12): 1118–1134.
- Holland, J.B., and Blundy, J.D. 1994. Non-ideal interactions in calcic amphiboles and their bearing on amphibole–plagioclase thermometry. *Contributions to Mineralogy and Petrology*, **116**: 433–447.
- Holland, T., and Powell, R. 1998. An internally consistent thermodynamic data set for phases of petrological interest. *Journal of Metamorphic Geology*, **16**(3): 309–343.
- Horstwood, M.S.A., Foster, G.L., Parrish, R.R., Noble, S.R., and Nowell, G.M. 2003. Common-Pb corrected in situ U–Pb accessory mineral geochronology by LA–MC–ICP–MS. *Journal of Analytical Atomic Spectrometry*, **18**: 837–846.
- Hunt, P.A., and Roddick, J.C. 1990. A compilation of K–Ar ages; report 19. In *Radiogenic age and isotopic studies*, Report 3. Geological Survey of Canada Paper 89-02, pp. 153–190.
- Hunt, P.A., Roddick, J.C., and Canada, G.S. 1991. A compilation of K–Ar ages; Report 20. In *Radiogenic age and isotopic studies*, Report 4. Geological Survey of Canada Paper 90-02, pp. 113–143.
- Johnson, B.J., and Brown, R.L. 1996. Crustal structure and early Tertiary extensional tectonics of the Omineca Belt at 51 degrees N latitude, southern Canadian Cordillera. *Canadian Journal of Earth Sciences*, **33**(12): 1596–1611.
- Johnston, D.H., Williams, P.F., Brown, R.L., Crowley, J.L., and Carr, S.D. 2000. Northeastward extrusion and extensional exhumation of crystalline rocks of the Monashee Complex, southeastern Canadian Cordillera. *Journal of Structural Geology*, **22**(5): 603–625.
- Kohn, M.J., and Spear, F.S. 2000. Retrograde new transfer reaction insurance for pressure–temperature estimates. *Geology*, **28**: 1127–1130.
- Kretz, R. 1983. Symbols for rock-forming minerals. *American Mineralogist*, **68**: 277–279.
- Laberge, J.D. 2005. Geology of the Granby Fault, southeastern British Columbia: metamorphism and tectonic evolution. M.Sc. thesis, Department of Geology and Geophysics, University of Calgary, Calgary, Alberta.
- Laberge, J.D., Pattison, D.R.M., and Simony, P.S. 2004. Geology of the Granby Fault, an Eocene Extensional Fault in Southeast British Columbia. In *Geological fieldwork 2003*. British Columbia Ministry of Energy and Mines, Paper 2004-1, pp. 33–48.
- Little, H.W. 1983. Geology of the Greenwood map-area, British Columbia. Geological Survey of Canada, Paper 79-37.
- Little, H.W., and Thorpe, R.I. 1965. Greenwood map-area, British Columbia. Geological Survey of Canada, Paper 65-1, pp. 55–60.
- Liu, M., and Furlong, K.P. 1993. Crustal shortening and Eocene extension in the southeastern Canadian Cordillera; some thermal and rheological considerations. *Tectonics*, **12**(3): 776–786.
- Lowdon, J.A. 1961. Isotopic ages, Report 2 of Age determinations by the Geological Survey of Canada. Geological Survey of Canada, Paper 61-17.

- Mader, U.K., and Berman, R.G. 1992. Amphibole thermobarometry: a thermodynamic approach. *In* Current research, part E. Geological Survey of Canada, Paper 92-1E, pp. 393–400.
- Massey, N.W.D., MacIntyre, D.G., and Desjardins, P.J. 2003. Digital Map of British Columbia: Tile NM11 Southeast B.C. British Columbia Ministry of Energy and Mines, Geofile 2003-2.
- Mathews, W.H. 1964. Potassium–argon age determinations of Cenozoic volcanic rocks from British Columbia. *Geological Society of America Bulletin*, **75**(5): 465–468.
- Meldrum, A., Boatner, L.A., Weber, W.J., and Ewing, R.C. 1998. Radiation damage in zircon and monazite. *Geochimica et Cosmochimica Acta*, **62**(14): 2509–2520.
- Monger, J.W.H., Price, R.A., and Tempelman-Kluit, D.J. 1982. Tectonic accretion and the origin of the two major metamorphic and plutonic belts in the Canadian Cordillera. *Geology*, **10**(2): 70–75.
- Nichols, G.T., Berry, R.F., and Green, D.H. 1992. Internally consistent garnite–spinel–cordierite–garnet equilibria in the FMASHZn system: geothermobarometry and applications. *Contributions to Mineralogy and Petrology*, **111**: 362–377.
- Norlander, B.H., Whitney, D.L., Teyssier, C., and Vanderhaeghe, O. 2002. Partial melting and decompression of the Thor-Odin Dome, Shuswap metamorphic core complex, Canadian Cordillera. *Lithos*, **61**(3–4): 103–125.
- Parrish, R.R. 1990. U–Pb dating of monazite and its application to geological problems. *Canadian Journal of Earth Sciences*, **27**: 1431–1450.
- Parrish, R.R. 1992. Miscellaneous U–Pb zircon dates from Southeast British Columbia. *In* Radiogenic age and isotopic studies, Report 5. Geological Survey of Canada, Paper 91-02, pp. 143–153.
- Parrish, R.R. 1995. Thermal evolution of the southeastern Canadian Cordillera. *Canadian Journal of Earth Sciences*, **32**: 1618–1642.
- Parrish, R.R., Carr, S.D., and Parkinson, D.L. 1988. Eocene extensional tectonics and geochronology of the southern Omineca Belt, British Columbia and Washington. *Tectonics*, **7**(2): 181–212.
- Pattison, D.R.M., and Bégin, N.J. 1994. Zoning patterns in orthopyroxene and garnet in granulites; implications for geothermometry. *Journal of Metamorphic Geology*, **12**(4): 387–410.
- Pattison, D.R.M., Chacko, T., Farquhar, J., and McFarlane, C.R.M. 2003. Temperatures of granulite-facies metamorphism: constraints from experimental phase equilibria and thermobarometry corrected for retrograde exchange. *Journal of Petrology*, **44**(5): 867–901.
- Powell, R., and Holland, T. 1994. Optimal geothermometry and geobarometry. *American Mineralogist*, **79**(1–2): 120–133.
- Preto, V.A. 1970. Structure and petrology of the Grand Forks Group, British Columbia, Geological Survey of Canada, Paper 69-22.
- Price, R.A., and Carmichael, D.M. 1986. Geometric test for Late Cretaceous – Paleogene intracontinental transform faulting in the Canadian Cordillera. *Geology*, **14**: 468–471.
- Pyle, J.M., and Spear, F.S. 2003. Four generations of accessory-phase growth in low-pressure migmatites from SW New Hampshire. *American Mineralogist*, **88**(2–3): 338–351.
- Ranalli, G., Brown, R.L., and Bosdachin, R. 1989. A geodynamic model for extension in the Shuswap core complex, southeastern Canadian Cordillera. *Canadian Journal of Earth Sciences*, **26**(8): 1647–1653.
- Rhodes, B.P., and Cheney, E.S. 1981. Low-angle faulting and the origin of Kettle Dome, a metamorphic core complex in north-eastern Washington. *Geology*, **9**(8): 366–369.
- Roback, R., Schiarizza, P., Nelson, J., Fyles, J.T., Ferri, F., Hoy, T., Ash, C., and Danner, W.R. 1995. Late Paleozoic arc and oceanic terranes and their external relationships, southern Quesnellia, B2: Field Trip Guidebook. Geological Association of Canada – Mineralogical Association of Canada, General Meeting, Victoria, B.C., May 1995.
- Ross, G.M., and Parrish, R.R. 1991. Detrital zircon geochronology of metasedimentary rocks in the southern Omineca Belt, Canadian Cordillera. *Canadian Journal of Earth Sciences*, **28**(8): 1254–1270.
- Scammell, R.J., and Dixon, J.M. 1993. Structure, thermochronometry and thermobarometry of former middle crust in the southeastern Canadian Cordillera; a record of synchronous and late orogenic extension in a mountain belt. *In* Late orogenic extension in mountain belts; international meeting. *Edited by* M. Seranne and J. Malavieille. Bureau de Recherches Géologiques et Minières, Paris, France, pp. 172–173.
- Schaubs, P.M., and Carr, S.D. 1998. Geology of metasedimentary rocks and Late Cretaceous deformation history in the northern Valhalla complex, British Columbia. *Canadian Journal of Earth Sciences*, **35**(9): 1018–1036.
- Schaubs, P.M., Carr, S.D., and Berman, R.G. 2002. Structural and metamorphic constraints on ca. 70 Ma deformation of the northern Valhalla Complex, British Columbia; implications for the tectonic evolution of the southern Omineca Belt. *Journal of Structural Geology*, **24**(6–7): 1195–1214.
- Sevigny, J.H., Parrish, R.R., Donelick, R.A., and Ghent, E.D. 1990. Northern Monashee Mountains, Omineca Crystalline Belt, British Columbia: Timing of metamorphism, anatexis, and tectonic denudation. *Geology*, **18**: 103–106.
- Simonetti, A., Heaman, L.M., Hartlaub, R.P., Creaser, R.A., McHattie, T.G., and Bohm C. 2005. U–Pb zircon dating by laser ablation–MC–ICP–MS using a new multiple ion counting–faraday collector array. *Journal of Analytical Atomic Spectrometry*, **20**: 677–686.
- Simonetti, A., Heaman, L.M., Chacko, T., et al. 2006. In situ petrographic thin section U–Pb dating of zircon, monazite, and titanite using laser ablation–MC–ICP–MS. *International Journal of Mass Spectrometry*, **253**(1–2): 87–97.
- Spear, F.S. 1993. Metamorphic phase equilibria and pressure–temperature–time paths. Mineralogical Society of America. Monograph Series.
- Spear, F.S. 2004. Fast Cooling and Exhumation of the Valhalla Metamorphic Core Complex, Southeastern British Columbia. *International Geology Review*, **46**(3): 193–209.
- Spear, F.S., and Parrish, R.R. 1996. Petrology and cooling rates of the Valhalla Complex, British Columbia, Canada. *Journal of Petrology*, **37**(4): 733–765.
- Spear, F.S., Kohn, M.J., and Cheney, J.T. 1999. *P–T* paths from anatexis pelites. *Contributions to Mineralogy and Petrology*, **134**: 17–32.
- Steiger, R.H., and Jäger, E. 1977. Subcommittee on geochronology: Convention on the use of decay constants in geo- and cosmochronology. *Earth and Planetary Science Letters*, **36**: 359–362.
- Stevens, R.D., Delabio, R.N., and Lachance, G.R. 1982. Age determinations and geological studies, K–Ar isotopic ages, Report 15. Geological Survey of Canada, Paper 81-2.
- Stevens, R.D., Delabio, R.N., and Lachance, G.R. 1983. Age determinations and geological studies; K–Ar isotopic ages, Report 16. Geological Survey of Canada, Paper 82-2.
- Tempelman-Kluit, D.J. 1989. Geology, Penticton, British Columbia; Map 1736A. Geological Survey of Canada, Ottawa, Canada.
- Teyssier, C., and Whitney, D.L. 2002. Gneiss domes and orogeny. *Geology*, **30**(12): 1139–1142.
- Teyssier, C., Ferré, E., Whitney, D.L., Norlander, B., Vanderhaeghe, O., and Parkinson, D. 2005. Flow of partially molten crust and origin of detachments during collapse of the Cordilleran orogen. *In* High-strain zones: structures and physical properties. *Edited*

- by D. Bruhn and L. Burlini. Geological Society (of London), Special Publication 245, pp. 39–64.
- Thompson, A.B. 1976. Mineral reactions in pelitic rocks: I. Prediction of P - T - X (Fe–Mg) phase relations. II. Calculation of some P - T - X (Fe–Mg) phase relations. *American Journal of Science*, **276**: 401–424, 425–454.
- Tomkins, H.S., and Pattison, D.R.M. In press. Accessory phase petrogenesis in relation to major phase assemblages in pelites from Nelson contact aureole, southern British Columbia. *Journal of Metamorphic Geology*.
- Wanless, R.K., Stevens, R.D., Lachance, G.R., and Edmonds, C.M. 1968. Age determinations and geological studies; K–Ar isotopic ages, Report 8. Geological Survey of Canada, Paper 67-2a.
- Wanless, R.K., Stevens, R.D., Lachance, G.R., and Delabio, R.N. 1979. Age determinations and geological studies; K–Ar isotopic ages; Report 14. Geological Survey of Canada, Paper 78-2.
- White, R.W., Powell, R., and Holland, T.J.B. 2001. Calculation of partial melting equilibria in the system Na_2O – CaO – K_2O – FeO – MgO – Al_2O_3 – SiO_2 – H_2O (NCKFMASH). *Journal of Metamorphic Geology*, **19**(2): 139–153.
- Whitney, D.L., Teyssier, C., and Vanderhaeghe, O. 2004. Gneiss domes and crustal flow. *In* Gneiss domes in orogeny. *Edited by* D.L. Whitney, C. Teyssier and C.S. Siddoway. Geological Society of America, Special Paper 380, pp. 15–33.
- Wing, B.A., Ferry, J.M., and Harrison, T.M. 2003. Prograde destruction and formation of monazite and allanite during contact and regional metamorphism of pelites; petrology and geochronology. *Contributions to Mineralogy and Petrology*, **145**(2): 228–250.
- Yang, P., and Pattison, D.R.M. 2006. Genesis of monazite and Y-zoning in garnet from the Black Hills, South Dakota. *Lithos*, **88**: 233–253.